3.3 Adsorption of metals

3.3.1 Metals on metals

H. BRUNE

3.3.1.1 Introduction

The following chapter gives an account of our present experimental knowledge on the adsorption of metal atoms onto solid metal surfaces of well defined structure and chemical composition. Only chemically clean and structurally well prepared low index surfaces of single crystals are considered. The samples are composed of a single element. The metallic adsorbates are condensed on the surface from the vapor phase in an ultra-high vacuum (UHV) chamber. As adsorbate materials we consider all metallic elements, apart from alkalies, to which Chap. 3.2. of the present volume is devoted. According to the definition of *adsorbed layers on surfaces* given in Chap. 1 of the present volume we concentrate on coverages of up to one atomic monolayer (ML, 1 ML is defined as one adsorbate atom per substrate unit cell). We refer to the literature for issues related to multilayer thin film growth and epitaxy [82Bau, 82Voo, 84Bau1, 98Pim, 98Zha], to theory and experiment of island nucleation [73Ven, 84Ven, 87Ven, 98Bru, 00Pol], to thermodynamic growth modes [84Bau1], or to strain relief [97Kin] in thin films comprising more than one atomic layer in thickness. In the spirit of the Landolt-Börnstein Series the data compilation focuses on experimental results. In the case of adsorption energies of monomers on atomic terraces we list theoretical results derived from *ab-initio* calculations for comparison.

Adsorption of metals from the vapor onto solid metal surfaces starts with the condensation of metal atoms at their impact site, which is in most cases located on an atomically flat substrate terrace. The energy E_{ads}, by which they are adsorbed, is topic of Sect. 2. It has long been a debate whether the substantial energy associated with the adsorption of metal adatoms is transferred instantaneously to excitations of the substrate lattice, or whether the adsorbate performs transient, non-thermal, motion over a few lattice sites until its adsorption energy is dissipated. Sect. 3 is devoted to this so-called transient (non-thermal) motion. The atoms, once in thermal equilibrium with the substrate, perform thermally activated two-dimensional (2D) diffusion, an issue treated in Chap. 3.11 of the present volume. As the coverage is increased beyond a few isolated monomers, the adsorption energy can become coverage- and site- dependent due to adsorbate-adsorbate interactions, which might span over several lattice sites. These lateral interactions are treated in Sect. 4. The last Sect. 5 treats the structure of submonolayer islands and of the first monolayer. Depending on the lattice mismatch and on the stiffness of lateral adsorbate interactions as compared to the corrugation of substrate adsorption potential, the adsorbed layer is either pseudomorphic with the substrate or it forms weakly incommensurate phases. For many combinations of metallic elements there is a tendency towards an exchange of adsorbate atoms with substrate atoms. This site exchange can be followed by the dissolution of the adsorbate into the bulk or by the formation of surface alloys where mixing is confined to the first atomic layer. The tables of Sec. 5 include information on the exchange of single atoms and on whether adlayer, surface alloys, or bulk alloys are formed.

Acronyms of experimental methods

ABS	Atomic Beam Scattering
ADE	Adsorption Desorption Equilibrium
ADT	Adsorption Desorption Transient
AES	Auger Electron Spectroscopy
AFM	Atomic Force Microscopy
ARXPS	Angle Resolved X-ray Photoelectron Spectroscopy
FD	Field Desorption

cont.

FEM	Field Emission Microscopy
HEIS	High Energy Ion Scattering
LEIS	Low Energy Ion Scattering
FIM	Field Ion Microscopy
LEED	Low Energy Electron Diffraction
MEIS	Medium Energy Ion Scattering
PAC	Perturbed γ-γ Angular Correlation
PDI	Photoelectron Diffraction Imaging
PDMEE	Primary-Beam Diffraction Modulated Electron Emission
RHEED	Reflection High Energy Electron Diffraction
RBS	Rutherford Backscattering Spectroscopy
SEXAFS	Surface Extended X-ray Absorption Fine Structure
SPA-LEED	Spot Profile Analysis Low Energy Electron Diffraction
STM	Scanning tunneling microscopy
SXD	Surface X-ray Diffraction
TDS	Thermal Desorption Spectroscopy
UHV-SEM	Ultra High Vacuum Scanning Electron Microscope
XPD	X-ray Photoelectron Diffraction

Acronyms of computational techniques

DFT	Density functional theory
FP-LMTO	Full-potential linear-muffin-tin-orbital
GGA	Generalized gradient approximation (for the exchange correlation)
LAPW	Linearized augmented plane wave (method)
LDA	Local density approximation (for the exchange correlation)

3.3.1.2 Adsorption energies

Condensation of metal atoms on metal surfaces is fairly simple, as compared to the chemisorption of molecules. There is no activation energy for adsorption (E_{ac} = 0 in Eq. (23) of Chap. 1) and consequently the metal atoms approaching the surface are directly attracted towards the adsorption minimum. The adsorption energy E_{ads} is of the order of a few eV/atom and thus bonding is substantial. The absence of E_{ac} and the high value of E_{ads} lead to temperature independent sticking coefficients of s = 1 up to elevated substrate temperatures.

The adsorbates considered here range from the electropositive alkaline earth and rare earth atoms (Groups IIA and IIIA, for the Group IA alkali metals see Chap. 3.2) via the Group 1B atoms to *d*-electron metals. The electropositive adsorbates behave very much as alkali metals, although less pronounced. They form large dipole moments, detected by work function measurements, and generally have repulsive lateral interactions. For the earth alkalines, there is generally a sharp drop in the adsorption energy upon monolayer completion reflecting itself also in a drop of *s*. For the rare earths, whether there is a change in *s* upon monolayer completion depends on the elements; on W(110), e.g., Eu shows a change whereas Gd and Tb do not [86Kol2]. For the *d*-electron metals, the adsorbate-substrate bond is of the same covalent nature as the adsorbate-adsorbate bond. Nevertheless, there is a layer dependence of E_{ads} for heteroepitaxial metal systems, but the variations are small compared to the absolute values of E_{ads} and thus the sticking coefficient stays s = 1 independent of coverage for a large temperature regime.

On the atomic terraces there are competing adsorption sites. Single metal atoms favorize highly coordinated hollow or sometimes even substitutional sites. For illustration of the adsorption sites and surface symmetry we show the low index surfaces of bcc, fcc and hcp crystals in Fig. 1. Only few experimental techniques directly reveal the adsorption site of single adatoms. Field ion microscopy (FIM) can accomplish this for refractory metals, which are strongly enough bound to sustain the imaging field. Scanning tunneling microscopy (STM) has also been used to reveal adsorption sites, which is not trivial as it requires simultaneous imaging of adsorbate and substrate with atomic resolution. Table 1 gives an

overview of the metal adsorption sites that have been unambiguously determined in the zero-coverage limit. Note that for Ir/Ir(111) single atoms adsorb preferably on stacking fault positions; the bulk stacking sequence is energetically favorable only for islands comprising a few atoms. This is not the case, however, for Pt/Pt(111) where fcc-sites are favored right away from the zero coverage limit on. Note also that STM-inferred adsorption sites are often substitutional sites or adatoms in troughs. For isolated adatoms on flat surfaces it is often impossible to unambiguously localize the adsorbate with respect to the substrate lattice. (One exception is the chemisorption system C/Al(111), where the hcp-site could be determined by simultaneous imaging of the two uppermost atomic substrate layers and of the adsorbate [90Bru]).

Due to adsorbate-adsorbate interactions, E_{ads} also depends on coverage. Ideally one would like to measure E_{ads} starting from isolated adatoms on terrace sites and then follow the evolution of E_{ads} all the way up to the completion of a monolayer. There are only a few ways to experimentally accomplish this. The first and most important is via the kinetics of desorption, which is only possible for systems with reversible adsorption, i.e., for heteroepitaxial systems that don't form bulk alloys (for binary phase diagrams see [58Han], for the tendency toward exchange and the stability of surface alloys see [97Chr]). In thermal desorption spectroscopy (TDS), or temperature programmed desorption (TPD), the surface is heated at a constant rate (dT/dt) while monitoring the partial pressure of the desorbing species with a mass spectrometer. The heating rate is kept low as compared to the pumping rate. The desorption rate r_{des} is given by the following expression

$$r_{des} = dn/dt = -n^x \nu_{des}(\theta)\exp(-E_{des}(\theta)/kT) , \quad (1)$$

where E_{des} is the activation energy for desorption and ν_{des} its attempt frequency. The desorption order is $x \in \{0;1\}$ for metals/metals, n is the density of adatoms, $n = \theta_s n_0$, with n_0 being the density of substrate atoms per m^2, θ_s is the adsorbate coverage expressed with respect to n_0. The absolute desorption rate in Eq. (1) is obtained by multiplying r_{des} with the sample area seen by the mass spectrometer.
Quantitative determination of $\nu_{des}(\theta)$ and $E_{des}(\theta)$ requires analysis of desorption curves for a series of different initial coverages using Eq. (1). This is the "model-independent" or "complete" analysis of TDS data [74Bau, 75Bau, 75Fal, 75Kin, 84Hab]. Frequently the following more simple procedure has been applied to derive an estimate for E_{des}. For submonolayer to monolayer coverages r_{des} has a single desorption peak located at T*. For first order desorption, which is often the case for metal/metal systems, and under the simplifying assumption that ν_{des} and E_{des} are coverage independent, one can derive E_{des} directly from T* [62Red] via

$$E_{des}/kT^* = \ln(\nu_{des}\, T^*/(dT/dt)) - 3.64 . \quad (2)$$

However, this is a potentially dangerous way to proceed since ν_{des} contains an entropy term $\exp(\Delta S/k)$ which can change ν_{des} by several orders of magnitude as a function of θ. Also E_{des} depends on coverage, due to adsorbate-adsorbate interactions. Thus the E_{des} values solely derived from Eq. (2) are subject to systematic errors, such that, not only absolute values of E_{des}, but also coverage trends may come out wrong [87Nie]. Despite these systematic problems the simplicity of the linear relationship Eq. (2) found by Redhead, coupled with assumed constant prefactor, forms the basis of many analyses of TDS spectra.
At constant coverage, the activation energy for desorption derived from TDS equals the isosteric heat of adsorption since $E_{ac} = 0$ for the metal/metal systems considered here. Under adiabatic conditions the isosteric heat equals the calorimetirc heat of adsorption, which we label adsorption energy E_{ads}.

For systems showing no intermixing at all, desorption takes either place from a 2D gas of atoms on the atomic terraces, and/or from the phase boundary between this 2D-gas and 2D condensed islands. Accordingly, the TDS derived values correspond to the binding energy at ideal terrace sites and/or at step sites of adsorbate islands. In quantitative TDS experiments desorption from both phases can be discerned such that binding energies for both adsorption sites can be derived separately. This is illustrated in Fig. 2 for Ni desorption from a W(110) surface. There are two branches for $\theta < 0.4$ ML, the upper is caused by desorption from the 2D-gas–2D-solid interface and thus from steps; the lower is due to desorption from the 2D-gas and thus to terrace sites. The strong coverage dependence of ν_{des} and E_{des} is evident. The

increase of E_{des} with increasing θ is a signature for attractive adsorbate-adsorbate interactions (see Sect. 3). The data points are sufficiently numerous that a sensible extrapolation to the coverage limit of single adsorbed adatoms is possible. Table 2 lists the adsorption energies inferred from TDS. In favorable cases where a complete analysis has been performed and thus E_{des} (θ) data are available, we list the zero coverage extrapolation, a value at the intermediate coverages where E_{des} is often constant, and the value at saturation coverage. In the cases where only T* values have been reported we list these values and the reader may derive estimates for E_{des} from Eq. (2) using the experimental heating rate and assuming $\nu_{des} = 10^{13}$ Hz.

For some systems, even though they do not form bulk alloys, annealing can lead to the formation of so-called surface alloys, where mixing is confined to the first atomic layer [97Bes]. An example is Ag/Pt(111), where annealing to T = 600 K leads to the formation of a real mixture where small Ag clusters are dissolved in the first Pt layer (θ < 0.5 ML) and vice versa (0.5 ML < θ < 1 ML) [93Röd]. The E_{ads} values derived for this system consequently do not correspond to the adsorption energy of Ag atoms on ideal Pt(111) terraces but presumably to desorption from a Ag-Pt adatom gas or from substitutional sites.

A test of absolute binding energies derived from TDS can be accomplished for homoepitaxial systems or for multilayers by comparing the TDS-result to the tabulated vaporization energy of the corresponding element [78Wea]. It is illustrative to compare the cohesive energy E_{coh} with the vaporization energy. If both energies are equal, atoms evaporate directly from kinks since E_{coh} is the binding energy at kink sites. If there is a difference between both energies, desorption takes place from terrace sites and the energy difference can be associated with the adatom formation energy, i.e., the binding energy difference between terrace and step sites.
For Cu we find

$$E_{coh} - E_{vap} = 3.49 \text{ eV} - 3.16 \text{ eV} = 0.33 \text{ eV},$$

and for Al

$$E_{coh} - E_{vap} = 0.34 \text{ eV},$$

which compares well with computed values [96Stu].

For heteroepitaxial systems forming bulk alloys, the TDS method to derive E_{ads} is not applicable and the only experimental technique allowing to deduce adsorption energies is calorimetry. This technique has recently been established for single crystal surfaces [91Bor, 98Bro] and gives access to adsorption energies on terrace sites. Generally, these values are integrated over a coverage interval, however, when the calorimeter is operated with sufficient time resolution in combination with a pulsed doser, E_{ads} can also be measured as a function of coverage [97Yeo2]. However, measuring the temperature increase of a bulk single crystal sample upon adsorption of a few percent of a monolayer of atoms from the vapor is experimentally challenging. Therefore this technique has so far only been applied to measure heats of adsorption for chemisorbed molecules as CO, O_2 and hydrocarbons on a few selected metal surfaces [93Stu, 96Stu, 96Yeo, 97Yeo1, 97Yeo2], but not yet to measure metal/metal adsorption energies.

Other sources of adsorption energies are the TDS-related adsorption desorption transient (ADT) and adsorption desorption equilibrium (ADE) measurements which can equally be extrapolated to the zero-coverage limit [84Bau1]. Differences in TDS- and ADE-derived E_{ads}(0 ML)-values are often ascribed to a barrier to desorption which manifests itself only in the inherently non-equilibrium thermal desorption process, but not in the quasi-equilibrium isosteric heat of adsorption obtained from ADE [92Kim].

Finally, there is the field desorption (FD) technique where the required field for adatom desorption in a FIM is used to draw conclusions on E_{ads}. Absolute values are certainly due to systematic errors since the field considerably perturbs the electronic binding configuration. However, the variation of E_{ads} between different elements is believed to be correct. We show results for the 5*d*-elements on various low index surfaces of W in Fig. 3. It is seen that the Re-atom having the half-filled 5*d* shell has the highest binding energy, whereas E_{ads} decreases in a symmetric fashion for elements having fewer or more 5*d* electrons than Re, respectively. For lanthanides there is a similar behavior, Gd, with its half-filled 4*f* shell, is most strongly bound.

For comparison with experiment we list in Table 3 binding energies for terrace sites computed with *ab-initio* methods. This Table shows that the LDA approximation for the exchange correlation functional leads to strong overbinding. This is reflected in the much too large E_{coh}-value calculated for Al. An approximation for the exchange correlation doing well for high coordinated slab atoms can do less well for low coordinated atoms, and thus for the isolated atom, taken as reference when calculating total binding energies. The overbinding of LDA is mostly due to difficulties in describing the isolated atom, whereas it is believed to be more accurate for the energetics of the slab. The absolute values of E_{ads} derived from GGA are expected to do better but yet they have to be taken with care. Despite these difficulties, relative energy values derived from density functional theory can be quite precise, as seen by the accord between measured and computed diffusion barriers recently obtained even for close-packed metal surfaces (see the example of Pt/Pt(111) with $E_{m,exp}$ = 0.260±0.003 eV [98Kyu] compared with $E_{m,th}$ = 0.29 eV [99Fei]; in this example also the preference of fcc-sites for single atoms comes out right from theory, compare Tables 1 and 3). Therefore, at the present state, the computed E_{ads} values can predict the favored adsorption site, and by this discriminate exchange from surface adsorption (see case of Co/Cu(100) in Table 3 for which an exchange at low θ and an ad-layer at 1 ML has been calculated in agreement with experiment), but not yet its absolute binding energy. Absolute E_{ads} values for terrace sites can be derived for homoepitaxial systems from theoretical adatom formation energies and the experimental cohesion energy.

Table 1. Experimentally determined adsorption sites for single adatoms (ordered after substrate according to periodic table)

System	Site(s)	Observations	Method	Ref.
Au/Ni(110)	substitution	Au in 1st layer Ni rows	STM	[93Nie]
Au/Ni(111)	substitution	Au in phase with Ni lattice	STM	[96Hol]
Pd/Cu(100)	substitution	Pd in phase with Cu lattice	STM	[96Mur]
Ag/Cu(100)	substitution	Ag in phase with Cu lattice	STM	[96Spr]
Ag/Cu(111)	substitution	Ag in phase with Cu lattice	STM	[97Bes]
Pb/Cu(111)	substitution	Pb in phase with Cu lattice	STM	[94Nag]
W/W(111)	L/F	94% on L-site, 6% on F	FIM	[74Gra]
Pd/W(110)	S	3-fold coord. surface site S	FIM	[84Bau1]
W/W(110)	S	3-fold coord. surface site S	FIM	[84Bau1]
Re/W(110)	L	2-fold coord. bulk lattice site L	FIM	[80Fin]
Ir/Ir(111)	hcp/fcc	hcp favored by 16 meV [a])	FIM	[89Wan]
Re/Ir(111)	hcp	atoms move from 50% hcp 50% fcc to hcp by ann. to 200 K	FIM	[91Wan]
W/Ir(111)	hcp	atoms move from 50% hcp 50% fcc to hcp by ann. to 200 K	FIM	[91Wan]
Pd/Ir(111)	fcc	atoms move from 50% hcp 50% fcc to fcc by ann. to 60 K	FIM	[91Wan]
Co/Pt(111)	substitution	Co in phase with Pt lattice	STM	[99Lun1, 99Lun1]
Pt/Pt(111)	fcc/hcp	fcc favored by > 60 meV [b])	FIM	[96Göl]
Pt/Pt(110)-(1x2)	4-fold	hollow in missing row trough	STM	[97Lin]
Pt/Au(111)	substitution	Pt in phase with Au lattice	STM	[99Ped]
Au/Au(110)-(1x2)	4-fold	hollow in missing row trough	STM	[97Gün]

[a]) The two non-equivalent sites are discerned by the non-uniform intensity distribution in the FIM images leading to triangles which apex point along, $[2\bar{1}1]$ or in the opposite direction, for hcp- and fcc-sites, respectively. The preference for hcp-sites is unique to single atoms and small clusters; with increasing cluster size the Ir atoms occupy fcc-sites.

[b]) At 20 K deposition temperature both sites are occupied at random, upon annealing to 45 K hcp atoms diffuse onto fcc-sites. The binding energy difference is inferred from the threshold T for diffusion out of the two sites, and from the known migration barrier between fcc-sites.

Table 2. Adsorption energies (order according to periodic system, first priority substrate, second priority adsorbate).

System	E_{ads} [eV]	T* [K]	θ [ML]	Method	Ref.
Hg/Fe(100)	1.13±0.12			ADE	[81Jon]
Hg/Ni(100)	1.19±0.15			ADE	[87Jon]
Ag/Ni(111)	3.03±0.06 [f])		1	ADE	[00Mró]
	3.24±0.08 [f])		2		
Hg/Ni(111)	1.14			ADE	[90Sin1, 90Sin2]
	0.83		p(2x2)		
	2.07		($\sqrt{3}$x$\sqrt{3}$)R30		
Hg/Cu(100)	0.70±0.03		0, c(4x4)	TDS [h])	[92Kim]
	0.74±0.03		0, c(2x2)		
	0.5		0, c(2x2)	ABS	[90Dow]
Ni/Mo(110)		1435	1	TDS	[90He, 90Tik]
Cu/Mo(110)		1222	1	TDS	[90He]
Mg/Ru(0001)	2.4 [d])	883/787	0.2	TDS	[99Hua]
	2.0 [d])	830/730	1.0		
Ni/Ru(0001)		1350	1	TDS	[88Ber2]
Cu/Ru(0001)		1210	1	TDS	[85Yat]
Zn/Ru(0001)	1.6	620-720	0.1-1.3	TDS [c])	[92Rod2]
Pd/Ru(0001)		1410-1440	0-1	TDS	[92Cam]
Ag/Ru(0001)	2.49±0.05 [e])		0.0	TDS [a]) [b])	[87Nie]
	3.00±0.05 [f])		$\geq$ 0.2		[93Rod]
	2.3 - 2.7 [d])	900-1050	0-1	TDS	
Au/Ru(0001)	4.04±0.05 [e])		0.0	TDS [a]) [b])	[87Nie]
	3.58±0.07 [e])		0.5		[86Har]
	3.42±0.10		0.1	TDS [a])	
	4.15±0.10		0.6		
	3.63±0.10		1.0		
Au/Ru(1000)	3.6 [e])		0.1	TDS [a])	[95Pou]
	3.9 [e])		0.2-0.5		
Cu/Rh(100)		1262	1	TDS	[91Jia]
Hg/Ag(100)	0.63±0.03		0	TDS [g])	[92Kim]
	0.25±0.03		1		
Ni/Ta(110)		1520	1	TDS	[97Cha]
Cu/Ta(110)		1258	1	TDS	[97Cha]
Pd/Ta(110)		1540	1	TDS	[90Koe]
Fe/W(100)		1480	0-1	TDS	[90Ber]
Ni/W(100)		1480	0-1	TDS	[87Ber]
Hg/W(100)	2.15±0.12			ADE	[78Jon, 79Jon]
	1.91±0.14			TDS	
Fe/W(110)	4.1 [g])		0-1	TDS [b])	[90Ber]
	3.6±0.1 [e])		0-0.8	TDS [a])	[00Kol]
	4.1±0.1 [f])				
Ni/W(110)	4.24±0.06 [c])	1475	1	TDS	[87Ber]
	4.35 [e])		0	TDS [a])	[86Kol2]
	5.00 [f])		0.2-0.4		
	4.93 [e])		0.6		
Cu/W(110)	3.20 [e])		0	TDS [a])	[86Kol2]
	3.85 [e])		0.2-0.4		
	3.85 [f])		0.2-0.8		

System	E_{ads} [eV]	T* [K]	θ [ML]	Method	Ref.
Pd/W(110)		1510	1	TDS	[88Ber1]
	3.6±0.1 [e])		0	TDS [a])	[80Sch]
	4.1±0.1 [e])		0.6		
	4.1±0.1 [f])		0		
	4.4±0.1 [f])		0.8		
	4.2±0.1		1.0-5.0		
Ag/W(110)	2.80 [e])		0.0	TDS [a])	[86Kol2]
	3.35-3.55 [e])		0.2-0.8		
	3.55 [f])		0.15-0.9		
Au/W(110)	3.30 [e])		0.0	TDS [a])	[86Kol2]
	3.67 [e])		0.2		
	4.10 [e])		0.8		
Eu/W(110)	2.85 [e])		0.08-0.26	TDS [a])	[86Kol1]
	2.10 [e])		0.42		
Gd/W(110)	2.85 [e])			TDS [a])	[86Kol1]
Tb/W(110)				TDS	[86Kol1]
Co/W(111)		1480-1440	0.2-1.0	TDS	[95Gua]
Ni/W(111)		1480	< 1	TDS	[95Gua]
Ag/W(111)		1180	< 1	TDS	[95Gua]
Cu/Re(0001)	2.1 [f])		0.1	TDS [a])	[99Wag]
	3.4		0.8		
		1180	1	TDS	[92Rod1]
Pd/Re(0001)		1350-1500	0-1	TDS	[92Cam]
Ag/Re(0001)	2.57±0.08 [f])		0.01	TDS [a])	[98Sch]
	2.76±0.04 [f])		0.10		
	3.01±0.04 [f])		0.50		
	3.11±0.08 [f])		0.75		
Ag/Pt(111)	2.88	1080	1	TDS [c])	[82Dav]
	2.63	970	≥2		[82Dav]
	3.2		0.0	TDS [a])	[86Har]
	4.1		0.6		
	3.6		1.0		

[a]) Complete analysis of a family of desorption curves with different initial coverages.
[b]) Excellent agreement is obtained for E_{des} from multilayers with bulk heat of vaporization.
[c]) ln r_{des} vs. $1/T$ analyzed, but no θ-dependence given.
[d]) Application of Eq. (2) and assumption of ν_{des} = 1x10^{13} Hz.
[e]) Desorption from 2D gas, E_{ads} on terrace site.
[f]) Desorption from interface between 2D gas – 2D solid adsorbate islands, E_{ads} on step.
[g]) Arrhenius behavior of leading edge was analyzed.
[h]) Simulation of TDS-spectra with exponential mobility model; this analysis also yields lateral interaction energies, e.g., for Hg/Cu(100)-c(4x4) $E_{des} = E_0 - \theta W$ with W = -0.13 eV, indicative of attractive lateral interactions. The results on E_0 and W are strongly model dependent; this is not included in the error bars above.

Table 3. Computed adsorption energies at terrace sites

System	E_{ads} [eV]	Site(s)	$E_{coh}/E_{coh\text{-}th.}$	θ [ML]	Slab *x* x *y* x *z*	Method	Ref.
Al/Al(111)	3.06/3.10	fcc/hcp	3.39/4.15	<1/9	>3x>3x5 [d])	DFT-LDA	[96Stu]
	x/x+0.04	fcc/hcp		1/56	14x4x6 [e])	DFT-LDA	[00Bog]
Al/Al(100)	3.75	4-fold	3.39/4.15	1/16	4x4x7 [d])	DFT-LDA	[96Stu]
	3.03	4-fold		?	?x?x2 [b])	LDA	[87Fei]
	2.93	4-fold		?	?x?x5	LDA	[90Fei]
Al/Al(110)	3.89	4-fold	3.39/4.15	1/12	3x4x8 [d])	DFT-LDA	[96Stu]
Ag/Ag(111)	2.82/2.84	fcc/hcp		1.0	1x1x5 [a])	FP-LMTO	[95Boi]
Ag/Ag(100)	2.99	4-fold		1.0	1x1x5 [a])	FP-LMTO	[95Boi]
Ag/Pt(111)	2.94	fcc		?	?x?x7 [d])	FP-LDF	[94Fei1]
Au/Au(111)	3.33/3.31	fcc/hcp		1.0	1x1x5 [a])	FP-LMTO	[95Bo]
Au/Au(100)	3.71	4-fold		1.0	1x1x5 [a])	FP-LMTO	[95Boi]
Cu/Cu(111)		fcc	hcp unstable	1/48	12x4x4 [d])	DFT-GGA	[00Bog]
Co/Cu(100)	3.92/5.25	4-fold/exch		0.1	2x2x7 [d])	LDA-LAPW	[00Pen]
	5.38	4-fold		1.0	2x2x7 [d])	LDA-LAPW	[00Pen]
Ir/Ir(111)	7.68/7.69	fcc/hcp		1.0	1x1x5 [a])	FP-LMTO	[95Boi]
Ir/Ir(100)	9.07	4-fold		1.0	1x1x5 [a])	FP-LMTO	[95Boi]
Pt/Pt(111)	5.35/5.17	fcc/hcp		?	?x?x7 [d])	FP-LDF	[94Fei1]

[a]) rigid slab
[b]) 1. layer relaxed in *z*-direction but kept rigid in *xy*-plane
[c]) 1. layer relaxed
[d]) 1. and 2. layer relaxed
[e]) first 4 layers relaxed

3.3.1.3 Atom condensation

3.3.1.3.1 Transient mobility

A metal atom approaching a metal surface from the vapor is captured by the strongly attractive adsorption potential and attracted by it towards the surface where it gains a binding energy of several electron volts. Transient mobility is the motion of atoms in the course of the dissipation of this adsorption energy. The possibility of this non-thermal motion between the initial site of impact and the final adsorption site has frequently been addressed in the literature since the early days of FIM investigations of atomic diffusion [64Ehr, 65Gur, 65You]. This interest was perhaps motivated by intuition suggesting that the several electron volts gained upon adsorbing a metal atom onto a metal surface would lead to a few jumps onto adsorption sites adjacent to the impact point before eventually reaching thermal equilibrium with the substrate. However, up to now, direct experimental proofs for transient mobility do not exist for metal on metal condensation. In contrast, every atomic scale experiment performed to study transient motion in detail, clearly excluded this type of motion for metals/metals (for FIM results see the overview given in ref. [91Wan]). In the following we discuss quantitative experiments addressing the issue of transient mobility.

Experimental methods permitting direct conclusions on transient motion examine the outcome of adatom deposition onto a substrate held at very low temperatures where thermally activated diffusion is frozen. This leads to statistical growth if transient mobility is absent, if present deviations from statistical growth are detected. In FIM experiments the population of adsorption sites is examined, whereas in STM experiments one measures the mean island size or island distance- and size-distributions.

FIM experiments can distinguish fcc- from hcp-adsorption on trigonal lattices [89Wan]. For Pt/Pt(111) these experiments revealed that the fcc-site is energetically favored by at least 60 meV (see Table 1) and therefore annealing of monomers to 45 K, promoting their thermal motion, leads to exclusive adsorption onto these sites. However, deposition at 20 K, where thermal motion is frozen for this system, led to adatoms randomly distributed over hcp- and fcc-sites [96Göl]. This implies that transient motion is absent since any mobility would lead to a preferred population of the energetically more favorable fcc-sites. Analog observations have been made for Ir, Re, W, and Pd on the Ir(111) surface (see Table 4).

STM measurements allow the determination of the mean island size $\langle s \rangle$ as quotient of coverage and island density. Both numbers are known with sufficient absolute precision that conclusions on transient mobility can be reached. This is achieved by experimentally following the mean island size with increasing coverage and making comparison to numbers expected from models for presence and absence of transient motion. The mean island size expected for the various lattice types for pure statistical growth can be estimated from percolation theory [76Syk1, 76Syk2]. However, this estimate yields slightly too small values since percolation theory neglects deposition onto filled sites. In kinetic Monte-Carlo (KMC) simulations one can account for impingement onto, and subsequent downward diffusion from islands or monomers. Such simulations yield $\langle s \rangle = 1.48$ atoms (percolation theory yields 1.35 atoms) *without*, and $\langle s \rangle = 2.3$ atoms *with* transient motion over one lattice site (values for $\theta = 0.1$ ML on a triangular lattice). This difference is clearly outside the experimental error bars and allowed to rule out transient mobility for Ag/Pt(111). Similar conclusions have been drawn from STM images acquired for Ni and Au/Au(110), where transient motion was excluded based on the chain lengths and distances, and on island size distributions, respectively (see Table 4).

There are diffraction experiments, from which transient motion has indirectly been concluded. RHEED-oscillations suggested 2D growth of Fe and Cu/Ag(100) at 77 K [89Ege] and diffraction rings implied a mean-island spacing of 10 atoms for Fe, Co, and Cu/Cu(100) at 80 K [93Nyb]. These observations are suggestive of transient motion. Nevertheless, explanations of these observations without the assumption of transient motion have been put forward in the literature [90Eva, 91San] such that these diffraction results cannot be considered as hard evidence for transient motion.

From the compilation of data in Table 4 we can conclude that transient mobility is precluded for all systems where direct atomic-scale observations exist. These results therefore suggest that generally for metals/metals the adsorption energy is instantaneously transferred to the substrate lattice and adatoms thermalize and condense at their impact point. The only exception is a "knock-on" exchange process

observed for Ir/Rh(100) by means of FIM [96Kel]. For this system thermally activated exchange sets in at 330 K, however, a fraction of 10% of the Ir atoms already exchanged with Rh at low *T*. This can be interpreted as transient vertical motion, i.e., part of E_{ads} is used to overcome the energy barrier of exchange.

Table 4: Experimental investigations of transient motion (TM, order periodic table for substrate)

System	TM	*T* [K]	Observations	Method	Ref.
Fe/Cu(100) Co/Cu(100) Cu/Cu(100)	+ [a])	80	diffraction rings	SPA-LEED	[93Nyb]
Ir/Rh(100)	+	77	10% ballistic exchange at 77 K, thermal exchange starts at 330 K	FIM	[96Kel]
Fe/Ag(100) Cu/Ag(100)	+ [a])	77	RHEED-oscillations -> 2D-growth	RHEED	[89Ege]
W/W(111)	- -	15	random distr. over different biding sites condensation on-top of 3-atom-sized W(111) plane	FIM FIM	[80Fla] [86Fin]
Pd/Ir(111)	-	20	random distr. over fcc and hcp sites	FIM	[91Wan]
W/Ir(111)	-	20	random distr. over fcc and hcp sites	FIM	[91Wan]
Re/Ir(111)	-	20	random distr. over fcc and hcp sites	FIM	[91Wan]
Ir/Ir(111)	-	20	random distr. over fcc and hcp sites	FIM	[91Wan]
Ag/Pt(111)	-	35	<*s*> shows absence of trans. mob.	STM	[99Bru]
Pt/Pt(111)	-	20 45	atoms randomly on hcp and fcc atoms solely on fcc-sites	FIM	[96Göl]
Ni/Au(110)	-	130	Ni chain length and spacing	STM	[97Hit]
Au/Au(110)	-	125	comparing experimental and theoretical cluster size distributions	STM	[97Gün]

[a]) Only indirect evidence for transient motion.

3.3.1.3.2. Neighbor-driven mobility

Apart from the absence of transient motion upon adatom condensation inmidst of flat terraces there are several observations suggesting that the motion of an adatom towards a neighboring adatom or island is different from thermal diffusion of isolated adatoms.

Wang and Ehrlich reported denuded zones, bare of Ir atoms, around Ir islands on Ir(111) [93Wan1, 93Wan2]. In the first set of FIM experiments Ir was condensed at 20 K and subsequently its diffusion was followed after annealing periods at 105 K. Far away from the island, atomic jumps could be traced in the usual way, but as soon as the lateral distance to the island was less than 3 nearest neighbor spacings, the atom was "funneled" in a single diffusion event toward the island [93Wan1]. In a second experiment the same group observed the denuded zones to be somewhat narrower (2 atoms wide) but to persist down to 20 K, i.e., in the absence of regular terrace diffusion [93Wan2]. These observations were interpreted as follows. Adatoms are stronger bound to ascending steps than they are at terraces. Therefore, the adatom adsorption potential becomes pulled down upon approaching a step, which also reduces its corrugation for motion toward the step, see Fig. 4. While the first set of data can be reconciled by a 10% reduction of the diffusion barrier, the depletion at 20 K would imply a reduction of that barrier by a factor of five! This reduction seems large for attachment to a one-fold coordinated step site. At this site the binding energy is increased by approximately the dimer bond energy of 0.32 eV [90Wan]. This can reduce the terrace diffusion barrier of 0.27 eV [89Wan] over a distance of two sites down to 0.19 eV (Fig. 4a), which is not sufficient to explain the observed motion at 20 K. Two- or three-fold lateral coordination to step atoms increases the binding energy approximately by 0.61 and 0.76 eV, respectively [89Wan]. This pulls the diffusion barrier down over two lattice sites to 0.12 eV (Fig. 4b) and 0.08 eV, respectively. However,

even the lower value of 0.08 eV is still too large to explain thermal motion at 20 K. One can only rationalize the FIM observations of denuded zones by thermal motion toward islands if strongly reduced barriers for the last few nearest neighbor distances are assumed. These barriers can not be attained by interactions pulling the potential linearly down over two sites. An alternative interpretation of the experiments would be transient motion toward the step over the strongly smoothened potential energy surface close to a step for the direction of step approach. A growth experiment at variable low temperature, as the one carried out by STM for Ag/Pt(111) (Table 4), would reveal whether and how much the barrier is reduced for motion toward monomers being one nearest neighbor distance apart. For Pd/Ag(100) He scattering experiments indicated such a "neighbor driven mobility" over one lattice site to be activated down to substrate temperatures of half the onset temperature of ordinary terrace diffusion [94Van]. This implies a reduction of the activation barrier for the attachment to an other monomer by a factor of two, as compared to the diffusion barrier for isolated adatoms.

The experiments of neighbor and island driven mobility could alternatively be explained as attraction of the atoms to neighbors or island step bottoms during their trajectory of arrival from the gas phase. However, such direct attraction to higher coordinated sites can be excluded for other systems as Ag/Pt(111), Au and Ni/Au(110) (see Table 4), which makes the explanation also unlikely for Ir/Ir(111) and Pd/Ag(100). Therefore, the currently most consistent interpretation is that metal atoms strike the surface perpendicularly, condense at the point of impact and then thermally diffuse. The adatom adsorption potential adjacent to other adatoms or islands is significantly smoothened for direction of approach by the increase in binding energy at laterally higher coordinated sites. Whether this smoothening suffices to explain the experimental observations of denuded zones and neighbor driven mobility reported so far remains to be clarified. Transient motion can alternatively be considered for the last one or two jumps toward monomers or islands over the smoothened potential energy surface, however, we emphasize that transient mobility is clearly excluded for individual monomers on the corrugated adsorption potential inmidst atomic terraces. The present discussion shows that while condensation of metal atoms onto terraces is well understood, their condensation close to steps and other adatoms is not yet as clear, encouraging further experimental and theoretical investigation. The details of the adsorption energy landscape in the vicinity of an island or a neighboring atom are expected to become relevant in the understanding of thin film and nanostructure growth.

3.3.1.4 Adsorbate – adsorbate interactions

The lateral interactions between adsorbed species play an important role in the formation of overlayers. They enter in their nucleation and growth as well as in the thermodynamically most stable structure taken on as function of coverage. Lateral adsorbate-adsorbate interactions have attracted theoretical [78Ein] and experimental [91Ehr] interest since decades. The interactions have several origins which can be divided according to the adsorbate separation. At small interatomic distances direct electronic interactions dominate and localized chemical dimer bonds are formed. This interaction falls off exponentially and is therefore of very short range. At larger separations adsorbate interactions are predominantly indirect and mediated in three ways: first electrostatically (dipole-dipole) and second elastically (deformation of substrate), which both decay monotonically with separation r as $1/r^3$, and third they are mediated by Friedel oscillations resulting from screening. Friedel oscillations are oscillations in the total substrate electron density around the adsorbates and lead to oscillatory interactions going as $\cos(2k_F r)/r^5$ for bulk electrons and as $\cos(2k_F r)/r^2$ for surface state electrons [78Ein, 78Lau, 00Hyl]. The important consequences of these laws are that surface state mediated interactions are expected to be of extremely long range, and that they oscillate with significantly larger wavelength than bulk electron mediated interactions since k_F(surface) >> k_F(bulk) (see, e.g., Ag where k_F((111)-surface state) = 0.083 Å^{-1} [99Jea] and k_F(bulk) = 1.2 Å^{-1} [87Ash]). Direct experimental evidence of long range surface state mediated interactions has very recently been obtained [00Kno, 00Rep].

In the following we treat adsorbate-adsorbate interactions. First for the simplest case of adsorbed dimers, and then we discuss the present knowledge on lateral interactions spanning over more than one lattice site.

3.3.1.4.1 Dimer bond energies

The experimental methods for determination of dimer bond energies and lateral interactions can be divided into those relying on indirect observations and those where adatoms or dimers are directly traced. In the first case integral techniques as TDS and $\Delta\Phi$, as well as local techniques (STM) have been used. In the case of TDS the dimer bond energies and/or lateral interactions are derived from the coverage dependence of the desorption energy. Often $E_{des}(\theta)$ is linear in coverage and written as $E_{des}(\theta) = E_{des}(\theta) - w\theta$. Thus $w > 0$ signifies attraction and $w < 0$ repulsion. Typical values for w derived in this manner are w = -0.41 eV/ML for Hg/Cu(100)-c(2x2) [90Dow] and w = 0.38 eV/ML for the denser (1x1) phase of Hg on the same surface [92Kim]. See also Hg on Fe(100) and on W(100) with w = 0.065±0.005 eV/ML [81Jon] and w = -0.092 eV/ML [78Jon, 79Jon], respectively. We note that these values stem from a macroscopic measurement and can not be associated to dimer or cluster bond energies. For some systems E_{des} does not vary linearly with θ but shows plateaus, as revealed by careful TDS experiments. It is believed that the levels of these plateaus correspond to the energy difference between atoms desorbing from the 2D adatom gas and those desorbing from the edges of adatom islands or small adatom clusters which coexist with the gas. An example was reported for Ag/W(110) by Kolaczkiewicz and Bauer [86Kol1]. The $E_{des}(\theta)$ data in Fig. 5 initially show a linear increase revealing attractive interactions between adatoms. At a coverage of 0.1 ML there is a first plateau, which has been associated with desorption from silver dimers leading to a dimer bond energy of 0.45 eV for that system. From similar observations, estimates of the dimer bond energies have been derived also for Ni, Cu and Au on W(110) (see Table 5). We note that the E_b-values derived that way are based on a particular view of what is happening on the surface - namely desorption from dimers - for which there is no direct substantiation. Assuming that the plateau corresponds to desorption from larger clusters would lead to smaller dimer bond energies - see trimer hypothesis and the values derived from Roelofs and Bellon cited in Table 5.

Interactions between adsorbates can lead to phase transformations in the adsorbed layer. At low coverages and high temperatures adatoms are expected to behave like a 2D lattice gas. If the coverage is increased, or the temperature lowered, one expects the formation of a condensed phase coexisting with the 2D lattice gas. Since the dipole moments per atom decrease rapidly with increased lateral coordination work function measurements ($\Delta\Phi$) clearly discern the monomer gas from the condensed phase. Therefore $\Delta\Phi$-measurements can reveal the boundary line between coexistence and pure 2D gas in the phase diagram of the adsorbed layer. Kolaczkiewicz and Bauer were able to deduce this phase boundary for Ni, Cu, Pd, Ag, and Au on W(110) [84Kol, 85Kol1, 85Kol2]. Their results for Ag/W(110) are shown in Fig. 6. The lateral interactions are inferred by fitting the experimental phase diagram with Monte Carlo simulations using nearest and next-nearest neighbor, as well as many atom interactions as input. Fig. 7 shows the pair and many atom interactions considered. Their large number gives rise to a multi-dimensional parameter space and it is likely that several points in this space may produce the observed phase diagram. This is suggested by the different results reported for the immediate nearest neighbor interactions by different authors, all analyzing the very same data shown in Fig. 6. Stoop obtains E_b = 0.074 eV [83Sto], which is much smaller than the value derived from TDS under the dimer hypothesis, whereas Ehrlich and Watanabe [91Ehr] obtain with the method from Roelofs and Bellon [89Roe] 0.18 eV. Kolaczkiewicz and Bauer derived pair interaction Lennard-Jones potentials from their $\Delta\Phi$ data [84Kol, 85Kol2], which yielded the E_b values marked as trimer hypothesis in Table 5 since they were derived under the assumption that desorption takes place from trimers [86Kol1]. This comparison for Ag_2/W(110) shows that macroscopic measurements can only be interpreted unambiguously if one knows what the rate limiting processes really are. This often requires information on the microscopic level.

Another indirect way to derive dimer bond energies recently evolved from variable temperature STM. The method relies on the fact that the density of nucleated islands is quite sensitive to the stability of small clusters. If the stable cluster changes from a dimer to a trimer, dimer dissociation enters in addition to monomer diffusion as a rate limiting step in cluster nucleation. Consequently, the Arrhenius plot of saturation island densities shows a marked change in slope as the dimer becomes unstable. Whereas the slope in the stable dimer regime only contains the monomer migration barrier, the slope at higher T contains in addition the dimer bond energy. Such nucleation studies have been carried out for only few

systems so far, however, they yield precise dimer bond energies (Table 5).
The experimental methods permitting direct exploration of monomer diffusion and dimer dissociation are FIM and STM. Dimer bond energies can be derived from FIM and STM by observing the dimer stability as a function of T. In the case of STM this has been done by determining the threshold temperature for the onset of 2D Ostwald ripening which yielded E_b = 0.15±0.02 eV for Ag/Pt(111), consistent with the nucleation results [99Bru]. STM has also been used to directly observe dimer association and dissociation events for Pt/Pt(110) [00Lin]. This study revealed that E_b is not exactly E_{diss} - E_m, as often assumed. A number of FIM studies explore the T-dependence of the dimer dissociation rate and derive E_b based on the known E_m values, using this assumption. Since the error of E_m also reflects itself in the one of E_b we only tabulate the recent E_b values, where E_m is known with high precision. For a review including also former studies see [91Ehr].

Table 5. Dimer bond energies (order after periodic table, first priority substrate and second adsorbate).

System	E_b [eV]	Method	Ref.
Cu/Ni(100)	0.46 ± 0.19 [a])	STM, nucleation	[96Mül1]
	0.34 ± 0.03 [b])	STM, nucleation	[98Bru]
Ni/W(110)	0.30	TDS	[86Kol1]
Cu/W(110)	0.35 [c])	TDS	[86Kol1]
	0.22 [d])		
	0.15	TDS	[75Bau]
	0.22	$\Delta\Phi$ data -MC analysis	[89Roe]
Pd/W(110)	0.18	FIM	[75Bas]
	(0.05-0.12/bond)	TDS	[80Sch]
	0.087±0.001	FIM	[99Koh]
Ag/W(110)	0.45 [c])	TDS	[86Kol1]
	0.18 [d])		
	0.074	$\Delta\Phi$ data -MC analysis	[83Sto]
	0.18	$\Delta\Phi$ data -MC analysis	[91Ehr]
Au/W(110)	0.35 [c])	TDS	[86Kol1]
	0.24 [d])		
	0.29	$\Delta\Phi$ data -MC analysis	[89Roe]
Re/W(110)	–0.032±0.009	FIM	[92Wat]
Ir/W(110)	0.065±0.003	FIM	[92Wat]
Ir/Ir(111)	0.32±0.02	FIM	[90Wan]
Ag/Pt(111)	0.15±0.02	STM, nucleation and Ostwald ripening	[99Bru]
Pt/Pt(110)	0.07±0.03	STM, $\nu_{diss}(T)$ and $\nu_{ass}(T)$ [e])	[00Lin]
Pt/Pt(111)	0.23±0.01	FIM	[99Kyu]

[a]) Deriving different ν_0 for monomer diffusion and dimer dissociation ($4 \times 10^{11\pm1}$ Hz and $5 \times 10^{12\pm2}$ Hz).
[b]) Assuming a common attempt frequency of $\nu_0 = 5 \times 10^{11\pm1}$ Hz for monomer diffusion and dimer dissociation.
[c]) Dimer hypothesis.
[d]) Trimer hypothesis.
[e]) Analysis of dimer dissociation and association rates show that $E_{diss} < E_m + E_b$ since E_m gets lowered for the last step towards another monomer (see discussion of neighbor driven mobility above).

3.3.1.4.2 Long range interactions

Long range adsorbate-adsorbate interactions can only be investigated by microscopic techniques. FIM has been used extensively for this purpose [91Ehr, 94Kel], and very recently also low temperature STM was applied [00Kno]. In both techniques the occupation of lattice sites by diffusing monomers close to another monomer or to an adisland is monitored as a function of temperature and time. Boltzman statistics then yields the differences in free energy between the different sites and thus one can in principle map out the atom adsorption potential. The results obtained with FIM show that the interactions are element specific, oscillatory, of several atomic distances in range, and they can be anisotropic. Instead of reviewing all interaction studies [91Ehr, 91Wat, 92Wat] we will only discuss a few examples to show the wealth of behavior found for different systems. For example, the atoms in a stretched Re dimer formed across adjacent atomic channels on W(211) repel each other at their smallest distance and attract each other if they are more than two neighbor distances apart. In contrast, two Re atoms positioned along one such channel on the same surface attract each other starting from 3 nearest neighbor distances until the dimer is formed [91Ehr]. The task of data recording and analysis becomes easier for heteropairs, since then, due to the different diffusion barriers, only one atom moves while the other atom stands still. The experiments of Watanabe et al., addressing Pd-Re on W(110), showed long range interactions, which were repulsive at short distances along [001] and [$1\bar{1}0$], and attractive along [$1\bar{1}1$] [91Wat]. The same trends as for Pd-Re were observed for W-Pd, for Ir-Ir [91Wat], and recently for Pd-Pd [99Koh]. A different behavior was observed for Re-Re where interactions are repulsive at close distances in all directions, attraction only begins to appear beyond 7.5 Å, but then it is again strongest along [$1\bar{1}1$] [92Wat]. These examples illustrate that the details of long range pair interactions vary from one atom to another, but the long range (> 10 Å) over which two atoms feel each other, and the orientational dependence, are common features.

The first STM results concerned with long range interactions revealed only indirectly that there was a long range repulsion between metal adatoms. In several nucleation studies too large island densities were systematically observed for metal/metal systems with migration barriers below 0.10 eV [00Bar]. These island densities can only be reconciled with a standard attempt frequency for diffusion of $\nu_0 = 10^{13}$ s^{-1} if long-range repulsion between the diffusing monomers delays island nucleation and thus increases densities as compared to standard nucleation with purely attractive interactions [00Bog, 00Fic]. An STM study showing long range ordering of surface segregated impurities on Cu(111) already gave some evidence to the existence of long range interactions on fcc(111) surfaces [98Wah]. However, these studies showed atoms placed only at some of the expected neighbor distances. Recent observations directly revealed the existence of such long range interactions for Cu diffusion on Cu(111) [00Kno, 00Rep] and also for Co/Cu(111) as well as for Co/Ag(111) [00Kno]. The interactions were found to oscillate with $\lambda_F/2$ and thus to be mediated by the surface state electrons; the interaction strength was only in the meV range and decayed as $1/r^2$ [00Kno] as predicted from theory for mediation by a partly filled Shockley type surface state [78Lau]. The short range repulsion for Cu/Cu(111) has been predicted in recent large scale DFT calculations [00Bog].

3.3.1.5 Overlayer structure

Adsorbed layers on single crystal surfaces are generally strained due to their lattice mismatch with the substrate. These layers are commensurate (C) when the corrugation of the substrate potential acting on the adsorbed atoms is large compared to the stiffness of their lateral bonds. If the lateral bonds are dominant, an incommensurate (I) layer results. In this case the adlayer lattice forms moiré patterns with the substrate lattice, which might be rotated to minimize their energy [77Nov, 79McT, 84Doe, 85Doe]. For the intermediate case, i. e., when both interaction potentials become comparable, weakly incommensurate phases are observed. They consist of large areas, which are nearly commensurate, separated by relatively narrow domain walls where the strain resulting from the lattice mismatch is locally relieved. The situation can be more complicated if the substrate participates in the relaxation. Vertical buckling of the first few substrate layers, for instance, can lead to adatoms on bridge sites being lower than atoms on hollow sites and thus to an inversion of adsorption heights as compared to expectation [95Hwa, 96Nag]. Finally, the adatoms can perform exchange processes and thereby substitute substrate atoms. For bulk inmiscible elements the structures formed that way are surface alloys, which are confined to one monolayer. For adsorbates forming a bulk alloy with the substrate, alloy layers might form at the surface as metastable intermediates before dissolution of the adatoms into the bulk.

The interest in thin metal films on metal substrates is mainly due to the possibility of using the interaction with the substrate to stabilize and create crystallographic structures of the adsorbate elements, which are inexistent or only stable under elevated temperature or pressures in its bulk [85Pri]. The most famous example is the stabilization of fcc-Fe down to low temperature by the growth on Cu(100) [67Jes, 68Jes] (bulk Fe exists in the fcc-phase only from 1200 – 1650 K, otherwise it crystallizes in a bcc lattice).

Many experimental techniques are allowing access to the structure of overlayers. However, each technique only reveals certain aspects of it and complete structural knowledge generally only evolves from a combination of several techniques. Conventional LEED reports the surface periodicity, whereas LEED-IV-curves give access to the vertical height of the adsorbate and to relaxations in the first few substrate layers, as does glancing incidence X-ray diffraction. Real-space imaging with STM directly shows whether the periodic structures inferred from diffraction are caused by a superposition of stacking domains. Ion scattering (LEIS, MEIS, HEIS) can reveal the chemical composition of the first few layers, which allows to distinguish adlayers from alloys and to determine the chemical composition of the latter. For surface alloys this can also be done with careful STM measurements. STM also shows the morphology of islands. For instance, a monolayer of Co on Cu(111) can be present in the form of three atomic layer high islands, the lowest one of which is embedded into the first Cu(111) plane and the middle layer is surrounded by a Cu rim resulting from the extracted substrate atoms [97Ped]. Such information can hardly be obtained from diffraction techniques – LEED only shows a (1x1) pattern for Co/Cu(111). On the other hand, the exact vertical positions of ad- and substrate atoms in an overlayer can only be deduced from diffraction experiments and their comparison with models. Valuable input for these models can come from STM images. Altogether, only the complementary use of several techniques unravels the entire structural information. For reasons of space, we will restrict ourselves in the Tables below to the lateral positions of the atoms. We will report if and from which temperature on there is exchange, but we will not table the exact vertical positions of the adatoms, which have been deduced for a few cases from LEED-IV or X-ray diffraction.

Before presenting the Tables, we now discuss typical examples of monolayer structures illustrated in Figs. 8 - 14. The trivial case is a pseudomorphic overlayer realized for small misfit *m* and/or for substrates with highly corrugated adsorption potential. The example reproduced in Fig. 8 shows a monolayer of Cu strained by 5.8% into registry with the Ru(0001) lattice. (Note that the strain *s* is defined with reference to the lattice constant of an adsorbate bulk plane with corresponding symmetry, in our case

s = (2.70 Å - 2.55 Å)/2.55 Å,

whereas the misfit *m* is defined with respect to the substrate, i.e.,

m = (2.55 Å - 2.70 Å)/2.70 Å = -5.5%).

The STM image of Cu/Ru(0001) reveals an atomic arrangement with a periodicity and symmetry identical to that of the substrate, the image is bare of long-range height modulation by which a weakly incommensurate phase would manifest itself.

For systems with large misfit, or with relatively stiff lateral bonds as compared to the corrugation of the adsorbate-substrate potential, there are several ways to accommodate strain in weakly incommensurate phases. These are shown for the case of hexagonally close-packed substrates in Fig. 9. These substrates have the unique property of two highly coordinated adsorption sites, the fcc and hcp hollows sites, whereas for instance on a square lattice there is only one four-fold hollow site. Therefore on hexagonal surfaces strain relief can proceed through formation of fcc- and hcp- stacking domains separated by domain walls, also called surface partial dislocations. The textbook example for strain relief by stacking transitions is the Au(111)-reconstruction where, driven by the tensile stress, a 4% compression of the first layer is achieved by two domain walls per $(\sqrt{3}\text{x}22)$-unit-cell, each inserting one-half extra atom, thus leading to 23 atoms adsorbed on 22 second-layer atoms along the close-packed $[1\bar{1}0]$-directions [85Har, 85Tak, 90Bar, 91San]. Due to the difference in binding energy more fcc- than hcp-sites are populated giving rise to a pairwise arrangement of the $[11\bar{2}]$-oriented domain-walls. Locally the compression is unidirectional, however, on large terraces a mesoscopic order of the domain walls is established: The domain walls bend by ±120° with a period of 250Å [90Bar] forming the so called herringbone structure which reduces the anisotropy of the surface stress tensor [92Nar]. The herringbone structure is schematically shown in Fig. 9a. Examples for such incommensurate striped phases (IS) of metal monolayers are Ag and Au/Ru(0001) and Ag/Pt(111) (see Fig. 10a).

Isotropic strain relief is achieved on a smaller length scale by trigonal networks as shown in Figs. 9b and c. These trigonal incommensurate phases (TI) involve domain wall crossing which can be costly due to their generally repulsive mutual interaction [79Bak], and due to the fact that the crossing points often involve unfavorable on-top adsorption sites. The threading dislocations shown in Fig. 9b are realized in the system Ag/Ru(0001) for $\theta < 0.85$ ML [95Ste], or for the alloy formed by Al on Au(111) [97Fis]. The trigonal network shown in Fig. 9c has so far only be seen for films comprising two or more monolayers (for strain relief and orientational relationships in multilayers, which is not the subject here, we refer to [97Kin, 98Zha] and to [82Bau], respectively). Both TI-phases (Figs. 9b and c) exhibit different areas of fcc- and hcp-stacking and thereby account for the energy difference of these two lattice sites. In the case shown in Fig. 9b this is realized by bending of the DL's forming convex (larger) fcc-areas and concave (smaller) hcp-areas. For straight DL's (Fig. 9c) different areas of the two stacking domains are created by shifting one class of domain walls relative to the crossing point of the two others; this also avoids crossing of all three domain walls in a single point [94Bru] (see 2. ML areas in Fig. 10b for an example).
Figure 10b shows a peculiarity of the system Ag/Pt(111) induced by the chemical potential of adatoms on-top of the first layer [97Bro]. A full Ag monolayer is pseudomorphic as seen in Fig. 10b by the absence of DL's in the first monolayer region. This is highly counterintuitive. The domain walls present in islands (Fig. 10a) should persist up to a full layer since the stress caused by lattice misfit is larger in a full monolayer than in adatom islands where stress can partly be relieved at the edges [97Bro]. Ag is under compressive stress on Pt(111) (m = 4.3%) and therefore the partial surface dislocations (DL) represent areas of locally lower atomic density. Before completion of the first layer, second layer Ag islands form, and due to the low 2D vapor pressure of Ag, these adatoms islands are in equilibrium with a 2D adatom gas created by lateral evaporation from the islands at 300 K. These adatoms fill in the first-layer DL's to gain coordination at the cost of stress increase in this layer.

The structure of overlayers is certainly a function of the preparation conditions; these have to be included for sensible comparison of the literature. Ag/Cu(111) is an example where several metastable structures are created as a function of increasing deposition temperature. Figure 11 shows that this system forms a moiré overlayer (T_{dep} = 225 K), while deposition at 300 K leads to a trigonal lattice of dislocation loops in the underlying substrate, substitution takes place at 775 K deposition temperature [97Bes].

On square lattices the substrate adsorption potential is typically highly corrugated (see the large monomer diffusion barriers on square lattices compared to close-packed surfaces reported in Chap. 3.11 of the present Volume). Therefore the most frequent structure of metal adlayers on surfaces with 4-fold symmetry is a pseudomorphic (1x1)-unit-cell. However, also on square lattices there are mechanisms of strain relief. Despite the fact that there are no stacking domains on such lattices (see above), there is a mechanism of strain relief which resembles the one on close-packed lattices. Single atomic rows can shift by half a lattice constant as seen for 1 ML Cu/Ni(100) (m = 2.56%) in Fig. 12. Thereby atoms in this row are displaced onto bridge sites where they appear higher in the STM topographs. Bridge site adsorption

has less coordination to the substrate which is counterbalanced by an increase of lateral coordination from 4 to 6 and the energy gain associated with strain relief [96Mül2]. This mechanism of strain relief continues in thicker films of Cu/Ni(110). In the *n*-th monolayer *n*-rows are shifted leading to internal {111}-facets between the pseudomorphic and the shifted stacking areas.

On fcc(110) surfaces there are close-packed rows in the $[1\bar{1}0]$-direction whereas the interatomic distance is $\sqrt{2}$-times as much in the [001]-direction. This open structure can lead to (1x2)-reconstructions for the clean surfaces where they rearrange into small close-packed {111}-facets. Substrate atoms in the uppermost rows are possible candidates for exchange processes as substantiated by the observation that diffusion on these surfaces often involves exchange (diffusion takes place by exchange on fcc(110) surfaces, e.g., for Pt/Ni(110) [91Kel], Au/Ni(110) [93Nie], Ir/Ir(110) [91Che], Re/Ir(110) [92Che], and W/Ir(110) [80Wri], for more examples see Chap. 3.11). In addition, many of the investigated heteroepitaxial metal systems with fcc(110) surfaces involve substitutional atoms as thermodynamically stable adsorbate structures (see for instance Pd/Cu(110) and In/Cu(110), see Table 6 for references). Exchange is also realized in the overlayer structures of Pb formed on Cu(110) at room temperature (Fig. 13), however, due to the large lattice constant of Pb, atomic rows along the less dense packed direction of the substrate are replaced by close packed Pb rows. The p(4x1) adlayer is energetically practically degenerate with structures where one Cu-row is replaced by a Pb row. This degeneracy leads to a coexistence of ad- and substitutional structures involving p(8x1) and p(12x1) unit-cells [95Nag]. The exchange on fcc(110) substrates can even lead to so-called subsurface growth where the adsorbate grows in the second layer and is capped by substrate atoms during deposition [92Rou, 97Hug, 97Mur].

The surfaces of the refractive metals generally participate only little in the structure of the adlayer as much as relaxations (large elastic modulus) and exchange processes (large surface free energy) are concerned. Therefore they often can be seen as a rigid surface onto which the adsorbate atoms accommodate for a given coverage in a way, which corresponds best to the lateral interactions between them and to the period and corrugation of the substrate adsorption potential. An example where adsorbate-adsorbate interactions are repulsive, much as for alkali metals (see Chap. 3.2), is Gd/W(110). This system stands for many rear earth elements on W surface and undergoes a sequence of commensurate structures with increasing adatom density as shown in Fig. 14.

In Tables 6-8 we have listed the submonolayer and monolayer structures of metals on the principal low index surfaces of metal substrates from 2- to 4-fold rotational symmetry. This compilation comprises heteroepitaxial systems only since the structure of homoepitaxial systems is in most cases trivial. For unreconstructed surfaces the bulk stacking is pseudomorphically continued and for reconstructed ones the reconstruction is lifted below the adlayer and at the same time taken on by the adsorbate layer. Only few homoepitaxial cases are worth mentioning since their reconstructions can metastably be lifted, as seen for Au/Au(110)-(1x2) [97Gün], or a reconstruction can be induced at a lower temperature by homoepitaxial adsorption, as seen for Pt/Pt(111) [93Bot].

We have only included systems, for which the original literature could be consulted by the author. For systems where several groups reported contradictory results, and these contradictions have now been removed, only the surviving truth is given and referred to; in cases where contradictions persist we list the different results. Due to the progress in surface science instrumentation and surface preparation during the recent decades clear preference is given to the more recent results. The former studies are often discussed and referred to in these more recent investigations. For references to the early literature, and for complementation of the Tables below, the reader may also consult the list of metal/metal structures given in the book of G. Somorjai [94Som]. The review article of E. Bauer [84Bau1] is also recommended as valuable collection of references, which partly complement the Tables given here on adsorption on refractory metals, in particular by references to the Russian literature.

Table 6. Overlayer structure on substrates with **2-fold rotational symmetry** (order according to periodic system, first priority substrate, second priority adsorbate)

System	Structure	θ [ML]	T_{dep}/T_{ann} [K]	Method	Ref.
Ni/Al(110)	intermixing NiAl	0-1	300	HEIS, XPS	[00Shu]
Cu/V(110)	(1x1)	0-2	300	LEED, XPS, AES	[99Kra]
Ag/Fe(110)	SK, 2 wetting ML	0-2	600	UHV-SEM	[96Nor]
Al/Ni(110)	3D islands	0-2	300	AES, STM, TDS,	[98Hah]
	dissolution into bulk		T_{an} > 600	AES	
Pt/Ni(110)	(1x1) [a])	0	> 105	FIM	[91Kel]
Au/Ni(110)	(1x1) [a])	< 0.5	570 [f])	LEIS	[95Dor]
	phase separation [b])	< 0.4	300	STM	[93Nie]
	(5x3)	> 0.4	300/700	STM, RBS	[95Nie]
		0.93	300		
Co/Cu(110)	(1x1) overlayer [c])	1.0	350	HAS	[98Töl, 99Töl, 00Töl]
	(2x2), c(2x4) alloy [c])	1.0		STM	[00Lin]
Pd/Cu(110)	Pd-Cu-chains	0	300	STM, theory	[97Mur]
	subsurface growth	> 0.1			
In/Cu(110)	substitution	10^{-4}	77	PAC	[89Kla]
Pb/Cu(110)	p(4x1) overl.	0.75	300	STM	[95Nag]
	p(4x1) [a])				
	p(9x1) [a])	0.778			
	p(5x1) [a])	0.80			
Fe/Mo(110)	(1x1)	0-1	300-370	STM	[00Osi]
Ni/Mo(110)	(2x8)			RHEED	[99Tsu]
Cu/Mo(110)	(1x1)	0-1		LEED	[84Bau2, 87Kol]
Pd/Mo(211)	chains along <111>	0-0.2	300	LEED	[98Ste]
	chain order (2x1)	0.2-0.5			
	chain order (3x1)	0.5-1			
Ag/Mo(110)	dist. hexagonal	0-0.8		LEED	[84Bau2, 87Kol]
Ba/Mo(110)	liquid	< 0.4	77	LEED, $\Delta\Phi$,	[98Gor]
	hex	0.6-0.7		EELS	
	c(6x2)	0.7			
	(2x3) and c(2x2)	0.09-0.26			
	close-packed hex	0.31			
	c(2x2), (1.6x2),	0-1	300/<900		[00Jo1]
	(1.5x1.8)			RHEED	
Pt/Mo(211)	chains along <111>	0-1	300	LEED	[98Ste]
	(1x1)		1300		
Pb/Mo(110)	$\begin{bmatrix} 10 & 0 \\ -3 & 4 \end{bmatrix}$	< 0.68	300-1000	RHEED, SEM	[00Jo2]
	$\begin{bmatrix} 1 & 0 \\ 1 & 3 \end{bmatrix}$	< 0.67	300-1000		
	$\begin{bmatrix} 1 & 0 \\ 3 & 10 \end{bmatrix}$	< 0.66	300-930		
	$\begin{bmatrix} 1 & -1 \\ 1 & 2 \end{bmatrix}$	> 0.33	1020-1070		

System	Structure	θ [ML]	T_{dep}/T_{ann} [K]	Method	Ref.
Ce/Mo(110)	$\begin{bmatrix} 7 & 0 \\ 1 & 2 \end{bmatrix}$	0-0.6	300	RHEED	[96Tan]
	$\begin{bmatrix} 5 & -1 \\ 1 & 2 \end{bmatrix}$				
	$\begin{bmatrix} 3 & 0 \\ 1 & 2 \end{bmatrix}$				
	$\begin{bmatrix} 0.62 & -1 \\ 1 & 2 \end{bmatrix}$				
Nd/Mo(110)	(14x2), (13x2), (11x2), (8x2), (6x2), c(6x2), c(4.5x2), c(5x3)	0-1	800	RHEED, AFM	[99Jo1, 99Jo2]
Au/Ru(1000) [d])	(1x1)	0.0-0.5	300	LEED	[95Pou]
	(1x3), Au-chains along [0100]	0.5-1.3			
Cu/Pd(110)	atomic Cu chains	0-0.1	250-300	STM	[94Buc, 97Li]
	pseudomorphic	0-1	< 600		[94Hah]
	intermixing		> 750		
Pd/Ag(110)	subsurface growth	> 0.1	300	STM, theory	[97Mur]
Au/Ag(110)	bilayer (1x1)	0.05-0.8	300	MEIS	[90Fen, 91Fen]
	subsurface growth	1.0	300	STM	[92Rou]
Ni/Au(110)	adatoms	0-1	130	STM	[97Hit]
	(1x2) surface alloy		300	STM,LEIS	[96Hug]
Cu/Au(110)	(1x2) subsurface growth	1	300	STM, LEIS	[97Hug]
V/W(110)	disordered	$\leq$ 1.0	300	LEED, AES,	[00Kol]
	surf. alloying		> 700	TDS, $\Delta\Phi$	
Mn/W(110)	(1x1) pseudom. [e])	1.0	300	STM, LEED	[99Bod]
Fe/W(110)	(1x1)	< 1.0	100/900	LEED	[90Ber]
	(10x10)	$\geq$ 1.0	100/720		
	epitaxial Fe(110) isl.		T_{ann} = 950		
	(1x1)	$\leq$ 1.1	300	LEED, AES, TDS, $\Delta\Phi$	[00Kol]
Co/W(110)	(1x1) 1-layer isl.	0-1	300/460	STM	[99Kah]
	relaxed 2-layer isl.	0-1	300/610		
	pseudomorphic with NW-orientation	0-1		LEED	[95Fri]
Ni/W(110)	(1x1)	$\leq$ 1.0	100	LEED	[87Ber]
Ag/W(110)	2 ML wet substr.	0-5	470-820	UHV-SEM	[83Spi]
Eu/W(110)	(3x2)	0.33	300	LEED	[86Kol1]
	(7x2)	< 0.43			
	hex	> 0.31			
	hex	< 0.53			

cont.

Table 6 (cont.)

System	Structure	θ [ML]	T_{dep}/T_{ann} [K]	Method	Ref.
Gd/W(110)	(10x2)	0.2	300/1200	LEED	[86Kol1]
	(8x2)	0.25	300/720	STM	[97Pas]
	(7x2)	0.29	300/1200	LEED	[86Kol1]
	(6x2)	0.33			
	(5x2)	0.40			
	c(5x3)	0.53			
	hex	0.64			
Ho/W(110)	random	≤ 0.1	300	STM, LEED	[00Pia]
	(*n*x2) stripes	0.1-0.5			
	moiré	0.5			

[a]) Adsorbate atoms substitute substrate atoms.
[b]) At 0.4 ML 0.16 ML Au that were initially alloyed into the Ni surface suddenly "pop out", for $\theta >$ 0.4 ML part of the Au is present in Au-chains forming on the Au-Ni alloy surface, part also goes back into the alloy surface such that $\theta_{chain}/\theta_{alloy} \approx$ const.
[c]) O acted as surfactant.
[d]) 1-fold substrate symmetry.
[e]) Stabilization of bcc δ-Mn up to a local thickness of 3 ML.
[f]) Adatoms were obtained by segregation from Ni(110) crystal containing 0.8% Au.

Table 7. Overlayer structure on substrates with **3-fold rotational symmetry** (order according to periodic system, first priority substrate, second priority adsorbate)

System	Structure	θ_s [ML]	T_{dep}/T_{ann} [K]	Method	Ref.
Fe/Al(111)	disordered alloy	0-1	300, 470	LEED-IV	[93Beg]
Ag/Al(111)	(1x1) [f])	1	300	LEIS	[00Los]
Sn/Al(111)	dense hex. overl.		300	LEED, AES	[80Arg]
Pb/Al(111)	dense hex. overl.	≤ 0.67	300	LEED, AES	[80Arg]
Cd/Ti(0001)	(1x1)			LEED-IV	[77Shi, 77Shi]
Mn/Co(0001)	ordered alloy	0.3-0.8	300	LEED	[98Cho, 99Cho1]
Pt/Co(0001)	(1x1)	0-1.0	300	LEED, XPS, STM	[00Cab]
Fe/Ni(111)	(1x1)	0-4	300	LEED, EELS	[00D'Ad]
Cu/Ni(111)	(1x1)	1.0	100/800	TPD, XPS	[00Kos]
Pd/Ni(111)	(13x13)-moiré	≤ 0.82	300	STM	[99Ter]
Ag/Ni(111)	moiré	0.74	300	STM	[97Bes]
	hex rot ±2°	0-2	180-900	AES, LEED	[00Mró]
Au/Ni(111)	substitution	0-0.1	500	STM	[96Hol, 98Bes]
	(9x9) moiré	0.79	170	STM	[95Jac]
	DL loops in Ni		300/400		
	surface alloy [k])	0.35-0.7	> 425	STM	[97Bes]
Hg/Ni(111)	$(\sqrt{3}x\sqrt{3})R30°$ p(2x2)			LEED	[90Sin1, 90Sin2]
Fe/Cu(111)	(1x1)	0-0.8	300/570	STM	[92Bro]
	(1x1)			LEED	[76Gra]
	intermixing [m])	0 – 1	300	STM, LEED	[00Pas]
	(1x1) fcc	0 - 1	300-350	SEXAFS	[00But]

System	Structure	θ_s [ML]	T_{dep}/T_{ann} [K]	Method	Ref.
Co/Cu(111)	substitution, Cu-capping	1.0	300/< 700	LEIS	[94Rab]
	Co-bilayer isl. and Cu-vacancy islands	0.6	300	STM	[93Fig]
	(1x1) Co- and Cu-termination	1.5	300	STM, LEED-IV	[96Fig]
	(1x1)-Co	1.0	150/300	STM	[97Ped]
	Cu-capping		300		
	pres. no exchange [n])	1.0	300	LEED-IV, STM	[00Pri]
Ni/Cu(111)	(1x1)			LEED-IV	[82Tea]
Pd/Cu(111)	(1x1)	0-1.0	300	LEED	[79Fuj, 83Pes]
Ag/Cu(111)	$\begin{bmatrix} 8 & 1 \\ 9 & -1 \end{bmatrix}$-moiré [l])	0.8	225	STM	[97Bes]
	DL-loops in Cu substitution	< 0.08	300 > 425		
In/Cu(111)	substitution	10^{-4}	77	PAC	[89Kla]
Sn/Cu(111)	$\begin{bmatrix} 2/3 & 2/3 \\ -2/3 & 4/3 \end{bmatrix}$ $\begin{bmatrix} 1 & -1 \\ 1 & 2 \end{bmatrix}$			LEED	[77Erl]
Te/Cu(111)	p(2x2) [a])	0.25	300/620	SEXAFS	[82Com]
Au/Cu(111)	(2x2)			LEED	[77Fuj]
Pb/Cu(111)	($\sqrt{3}$x$\sqrt{3}$)R30° [c])	0-0.21	300/523	STM	[94Nag, 96Nag]
	(2x2) [c])	0-0.21			
	(4x4)-Pb [d])	0.53			
Mg/Ru(0001)	(5x5)	0.64	300	LEED-IV	[96Sch]
	(7x7)	0.73			
Al/Ru(0001)	(1x1)	0-1	300	STM, $\Delta\Phi$, LEIS	[96Kop], [95Wu]
	surface alloy	1	600-1170		
Fe/Ru(0001)	(1x1)	0-1	200	AES, LEED, $\Delta\Phi$	[99Kol2]
	adlayer until des.	≤ 1.0	$T_{an} \leq 1200$		
Co/Ru(0001)	(1x1) pseudom.	≤ 1	300/600	STM, LEED	[93Vri]
Ni/Ru(0001)	(1x1) pseudom.	≤ 1.0	300	STM	[95Mey]
	part. DL loops	1.1-1.3			
	adlayer until des.	≤ 1.0	$T_{an} \leq 1100$	AES, LEED, $\Delta\Phi$	[99Kol2]
Cu/Ru(0001)	(1x1) pseudom.	≤ 1.0	300/500	STM	[95Gün]
			300	LEED	[87Par]
	DL loops	1.1-1.3	300/520	STM	[91Pöt]
Rh/Ru(0001)	(1x1)	≤ 1.0	300	AES, LEED, $\Delta\Phi$	[99Kol2]
	adlayer until des.				
Pd/Ru(0001)	(1x1)	< 1.0	350/500	LEED	[92Cam]
	pure adlayer until desorption		$T_{an} \leq 1100$	AES, LEED, $\Delta\Phi$	[99Kol2]
Ag/Ru(0001)	unidirectionally strained hex.	= 0.90	300	STM	[95Ste]
	buckl. of underl. Ru	≤ 0.85	300	STM	[95Hwa]
	threading DL's		300	STM	[95Ste]

cont.

Table 7 (cont.)

System	Structure	θ_s [ML]	T_{dep}/T_{ann} [K]	Method	Ref.
Pt/Ru(0001)	(1x1) adlayer isl.	< 0.5	T_{an} < 920	STM	[98Mon]
	surface alloy	0.4	300/1200		
Au/Ru(0001)	(1x1)	≤ 0.8	300	STM	[92Hwa, 92Sch]
	unidirextionally strained hex.	0.9	300/1200		
Mg/Pd(111)	only local order substitution	0-0.7	<250	XPD, LEED	[93Fis]
V/Pd(111)	V exchanges with 1. Pd layer, Pd isl.	< 0.5	300	STM, LEIS, XPD	[00Kon]
	($\sqrt{3}$x$\sqrt{3}$)R30° with 1. layer pure Pd 2. layer $V_{0.33}Pd_{0.66}$		570		
Fe/Pd(111)	(1x1), likely [c])	1	300, 570	LEED-IV	[93Beg]
Ag/Pd(111)	(1x1) [f, g])	1.0	300	ARXPS, LEED-IV	[93Eis]
Au/Pd(111)	(1x1) isl.	< 1	100-300	STM	[97Gle]
	(1x1) surface alloy		300/925		
Fe/Ag(111)	(1x1) [h])	1	300, 470	LEED-IV	[93Beg]
	island growth				
Ni/Ag(111)	substitution	0.1	300-500	STM	[95Mey]
	moiré islands with d_{nn} = 2.5 Å, α = 5.9°	0.1	130-285	STM	[98Hir]
Sb/Ag(111)	substitution [e])	0.08-0.3	300	STM	[98Veg]
Au/Ag(111)	substitution	1.0	300	ARXPS	[94Eis]
Tl/Ag(111)	($\sqrt{3}$x$\sqrt{3}$)R30° followed by moiré	≤ 0.70		LEED, RHEED, AES	[78Raw]
Pb/Ag(111)	($\sqrt{3}$x$\sqrt{3}$)R30° - isl.	0 - 0.33	300	TEM	[81Tak , 82Tak, 83Tak]
	R30° isl. coex. with moiré, α = ±(3 -5)°	0.33 - 0.67			
	R30° and moiré	≤ 0.67	300 - 400	LEED, RHEED	
	with moiré	0.67		LEED	[78Raw] [84Rol]
Fe/W(111)	(1x1)	1.0	300	LEED, AES, $\Delta\Phi$	[99Kol1]
Co/W(111)	(1x1)	1.2	T_{ann} > 1200	LEED	[95Gua]
Ni/W(111)	(1x1)	1.0	300	LEED	[95Gua]
				LEED, AES, $\Delta\Phi$	[99Kol1]
Cu/W(111)	(1x1)	0-1	300/1100	LEED	[95Gua]
Rh/W(111)	(1x1)	0.9	800-1300	LEED	[95Gua]
	{211}-subst faceting	1.0	T_{ann} > 900		
Pd/W(111)	(1x1)	1.0	300	LEED, AES, $\Delta\Phi$	[99Kol1]
Ag/W(111)	(1x1)	0-1.1	T_{ann} = 900	LEED	[95Gua]
Ir/W(111)	{211}-subst faceting	≥ 1.0	T_{ann} > 1100	LEED	[95Gua]
Pt/W(111)	{211}-subst faceting	0.3 - 2.0	T_{an} > 750	LEEM	[99Pel]
Ti/W(111)	(1x1)	0-1	T_{ann} < 1500	LEED	[95Gua]
Gd/W(111)	(1x1)	0 – 1	300-1500	LEED	[95Gua]
	no intermixing	0 - 1	300	FEM	[99Sha]
Co/Re(0001)	(1x1) with little intermixing	0 - 1	300	LEED, STM	[99Par]
	(2x2) surf. alloy in isl. and substrate		≥ 400		

System	Structure	θ_s [ML]	T_{dep}/T_{ann} [K]	Method	Ref.
Cu/Re(0001)	(1x1)	0-0.8	300	LEED, TDS, XPS	[99Wag]
	(14x14)	0.8-2.0	300/970		
Pd/Re(0001)	(1x1)	0-1	350/500	LEED	[92Cam]
Ag/Re(0001)	(1x1)	< 0.93	300-600	STM, LEED	[97Par]
Al/Pt(111)	adislands	< 0.5	300	STM	[00Lee]
	intermixing		T_{an} = 500		
	(2x2) Pt_3Al alloy		T_{an} = 800		
	dissolution of Al into Pt bulk		T_{an} > 1000		
V/Pt(111)	bcc(111) phase	1	300	XPD	[99Sam]
Co/Pt(111)	(1x1) adatom isl. on hcp and fcc sites	< 0.5	< 200	STM	[00Var]
	exchange induces Pt(111) reconstr.	> 0	300	STM	[95Grü, 99Lun1] [97Fer]
	fcc -> hcp		T_{ann} > 450	SXD	[95Atr, 97Fer]
	alloying		T_{ann} > 550		[94Grü]
	dissolution into bulk		T_{ann} > 750	STM, AES	[98Tsa, 99Hen]
	(10x10)	1.1	300	LEED	
Ni/Pt(111)	(1x1) pseudo	1	300	XPD	[98Sam]
Cu/Pt(111)	(1x1) adlayer	1	340	STM, HAS	[97Hol]
	exchange [j])	1	450	STM, HAS	[98Hol]
	alloy islands	< 1	600	STM	[00Sch1]
Pd/Pt(111)	(1x1)	0 - 1	300	LEED	[91Att, 94Att] see also [00Mar]
Ag/Pt(111)	(1x1) pseud. islands	0-0.5	300	STM	[97Bro]
	isl. ø > 200Å DL's	0.2-0.9			
	back to pseudomor.	1.0			
	surface alloy	0-0.99	$T_{ann} \geq 620$	STM	[93Röd, 93Str]
	surface alloy			PAX, HREELS	[00Fey]
La/Pt(111)	(1x1)	< 0.5	300/ <900	LEED, XPD	[00Ram]
	(2x2) surface alloy	> 1	300/900		
Re/Pt(111)	(1x1) adislands with edge alloy	0 - 0.8	300	LEED, XPS, STM	[99Ram]
	3-layer alloy		T_{ann} = 1000		
Al/Au(111)	adatoms	0.1	< 230	STM	[99Fis]
	exchange		> 230		
	surface alloy, distorted hex. phase	0.2	350/450	STM	[97Fis]
Fe/Au(111)	nucl. at elbows [i])	0.4-1	300	STM	[91Voi2, 92Str]
Co/Au(111)	subst. at elbows	$<10^{-3}$	300	STM	[96Mey]
	monolayer islands	10^{-3}-10^{-2}	300	HAS	[97Töl]
	bilayer islands	0.02-0.8	300	STM	[91Voi1]
	these sink by 1 layer		T_{ann} > 400	STM	[99Pad]
	Co diff. into bulk		T_{dep} > 450	HAS	[97Töl]
	dissolution into bulk		T_{ann} = 750	STM	[99Pad]
Ni/Au(111)	nucl. at elbows [i])	0.1-1	300	STM	[91Cha2, 93Cha]
Mo/Au(111)	nucl. at elbows	0.1	300	STM	[00Hel]

cont.

Table 7 (cont.)

System	Structure	θ_s [ML]	T_{dep}/T_{ann} [K]	Method	Ref.
Rh/Au(111)	coex. of 1 and 2-layer islands	0.2	300	STM	[94Alt]
	dissolution into bulk		T_{ann} = 670		
Pd/Au(111)	adatoms	0.1	150	LEIS	[92Koe]
	intermixing		300/240		
Ag/Au(111)	(1x1)	0-1	300	STM	[89Dov, 91Cha1, 93Cha]
	rec. locally lifted				
Pt/Au(111)	substitution	0.00 - 0.03	300	STM	[99Ped]
	mixed PtAu islands & subsurface Au isl.	0.03 - 1.0			
	pure Pt islands	> 1.0			
Pb/Au(111)	5% exp. 30° rot. Pd(111) - isl.	< 0.68		LEED, AES	[78Bib]
	moiré, α = 5°	0.68			
		$\leq$ 0.68		TEM	[82Tak]
Cu/Pb(111)	(1x1) subsurface isl.	0-3	300	STM	[95Nag]

[a]) Adsorbate atoms substitute substrate atoms.
[b]) O acted as surfactant.
[c]) Surface alloy.
[d]) de-alloying.
[e]) Sb segregation upon annealing or Ag deposition, this gives rise to surfactant effect of Sb in Ag growth.
[f]) 1. ML is pseudomorphic, i.e., continues the substrate stacking,
[g]) 2. layer grows with stacking fault.
[h]) LEED-IV-curves remain unchanged upon adsorption.
[i]) Likelihood of substitution at elbows leading to the observed heterogeneous nucleation.
[j]) Cu adlayer and exchange from the adlayer into Pt induces substrate reconstruction.
[k]) the lattice constant of the surface alloy changes smoothly with composition following Vegards law in 2D.
[l]) The STM images obtained after 300 K deposition by McMahon et al. [92McM] were falsely interpreted as (9x9) moiré pattern. After the study of Besenbacher et al. they are due to partial DL loops in the underlying Cu.
[m]) Intermixing can be suppressed with Pb as surfactant, also Fe is in fcc state up to 4 ML when Pb is used.
[n]) Presumably abrupt interface between Co and Cu when Pb is used as surfactant.

Table 8. Overlayer structure on substrates with **4-fold rotational symmetry** (order according to periodic system, first priority substrate, second priority adsorbate)

System	Structure	θ [ML]	T_{dep}/T_{ann} [K]	Method	Ref.
Sn/Al(100)	c(2x2)			LEED, AES	[78Arg1]
Pb/Al(100)	c(2x2)			LEED, AES	[78Arg1]
Fe/Cr(100)	ordered surf. alloy $Fe_{0.5}Cr_{0.5}$	0-0.5	300/470	STM	[99Cho2]
Cr/Fe(100)	disordered alloy with 0-0.1 ML surf Cr	0-1	570	STM	[96Dav]
Mn/Fe(100)	(1x1), bcc δ-Mn	1.0	570	MEIS, LEED	[97Pfa]
Co/Fe(100)	(1x1)	0-1	300	XPD	[93Zha]
				LEED, PDMEE	[00Ber]
Ni/Fe(100)	(1x1)	0-1	300	XPD	[93Zha]
Hg/Fe(100)	(1x1)	0-1		LEED	[81Jon]
Al/Ni(100)	(1x1) poor order Ni_3Al(100) alloy	1.0	300 > 300	LEED-IV	[88Lu]
Mn/Ni(100)	c(2x2) [c])	0.5	270	LEED-IV	[93Wut]
Fe/Ni(100)	(1x1) intermixing	0-1	300	PDMEE, LEED	[99Luc]
Cu/Ni(100)	(1x1) [e])	0-1	200-400	STM	[96Mül1]
Ag/Ni(100)	c(2x8) hexagonal	0.17-1.0	300	STM	[91Bro]
				LEED	[99Tod]
V/Cu(100)	(1x1)	< 0.5	300	LEED, XPD	[00Moo]
	(2x1)	0.5-1.5			
Cr/Cu(100)	(1x1)	1.0	300	LEED	[94Hau] [96Law]
	pseudom. 3D islands	0.5-3	285-575	STM	
Mn/Cu(100)	c(2x2) [c])	0.5	270/470	LEED-IV	[93Wut]
				MEIS	[99Bro]
Fe/Cu(100)	c(2x2) [c])	0.5	300	STM	[92Cha, 93Joh, 94Cha]
Co/Cu(100)	(1x1)	1.0		LEED	[68Jes, 83Mir, 84Fal]
	[b])	0		STM	[99Nou]
	Co-Cu alloy and pure Co coexisting	0-2	300 300	XPS, UPS, PAX, LEED	[00Kim]
Pd/Cu(100)	c(2x2) [c])	0.5	300	STM, LEED, RBS	[96Mur]
				LEED-IV	[88Wu]
	(2x2)p4g clock rec. [b])	1.0	300	MEIS	[96She1, 96She2]
Ag/Cu(100)	c(10x2) hex ad.-layer	= 0.9	250	STM	[96Spr, 97Bes]
		= 0.9	300/425		
	(1x1) surf. alloy coex. with c(10x2) layer in alloy layer	< 0.9	≥ 300		[67Bau, 68Pal]
	$\begin{bmatrix} 2 & 0 \\ -1 & 5 \end{bmatrix}$		300	LEED	[93Nak]
	c(2x10) hex		300/420	LEED, MEIS	
In/Cu(100)	substitution	10^{-4}	77	PAC	[89Kla]
Te/Cu(100)	$(2\sqrt{3}x2\sqrt{3})R30°$	0.33	300/620	SEXAFS	[82Com]
Pt/Cu(100)	c(2x2) [b])	1.0	300/470	LEIS, LEED	[96She]

cont.

Table 8 (cont.)

System	Structure	θ [ML]	T_{dep}/T_{ann} [K]	Method	Ref.
Au/Cu(100)	c(2x2) [c)]	0.5	300	LEED-IV	[87Wan]
				STM	[92Cha1]
				MEIS	[99Bro]
				PDI	[93Tob, 95Tob]
	c(14x2)	1.0	300	LEED, XPD	[93Nau]
				MEIS	[93Nak]
	de-alloying	1.2		MEIS	[96She]
Hg/Cu(100)	(3x3) & c(2x6)		120	LEED	[92Kim]
	c(2x2)	0.1 - 0.5	200		
	c(4x4)	0.2 - 0.62			
	$(\sqrt{2}x\sqrt{2})R45°$	0.5	300	LEED	[87One]
Tl/Cu(100)	$\begin{bmatrix} 2 & 2 \\ 2 & -2 \end{bmatrix}$	≤0.60	100-300	LEED	[91Bin]
	$\begin{bmatrix} 4 & 0 \\ 2 & 7 \end{bmatrix}$	0.67	300		
	$\begin{bmatrix} 6 & 6 \\ 2 & -2 \end{bmatrix}$	0.67	100		
Pb/Cu(100)	$(\sqrt{61}x\sqrt{61})R\tan^{-1}(5/6)$	0.1-0.5	150-250	HAS, LEED	[93Li]
	c(4x4) surf. alloy	0.38-0.45	250-450	LEIS	[98Pla]
	c(2x2) adlayer	0.45-0.53	250-450		
	$c(5\sqrt{2}x\sqrt{2})R45°$	0.57-0.68	250-450		
	consisting of		160–220	STM, LEED	[98Boc]
	antiphase domain-walls in c(2x2)		300/570	LEEM	[00Kel]
Bi/Cu(100)	dispersed	<< 0.67		LEED, AES	[78Arg2]
	dense hex. overlayer	0.67			
Al/Pd(100)	(2x2)-p4g bilayer surface alloy	0.5 - 2	300/700	STM, LEED	[00Kis]
				LEED	[00Oni]
Mn/Pd(100)	c(2x2) [c)]	0.5		LEED-IV	[90Tia]
Cu/Pd(100)	(1x1) pseudom. [f)]	0-1	300-400	STM	[95Hah]
Cr/Ag(100)	(1x1)	1.0		LEED	[94Hau]
Mn/Ag(100)	surf. alloy	0-3	300	SEXAFS	[99Sch]
	c(2x2)	0-1	210-340	LEED	[00Sch2]
Fe/Ag(100)	substitution	0.1	>130	LEIS	[97Lan]
Co/Ag(100)	adislands	0.1	275/425	STM	[00Deg]
	incorporated islands		425		
Pd/Ag(100)	substitution	0.1	>135	UPS	[96Pat]
	(1x1)				[82Smi]
Pt/Ag(100)	substitution	0.1	>200	UPS	[96Sch1]
Hg/Ag(100)	(1x1)	< 0.7	120	LEED	[92Kim]
Fe/W(100)	(1x1)	≤ 1.0	100/700	LEED	[90Ber]
Ni/W(100)	(1x1)	≤ 1.0	100	LEED	[87Ber]

System	Structure	θ [ML]	T_{dep}/T_{ann} [K]	Method	Ref.
Cu/Ir(100)	anisotropic Cu islands Ir chains from lifting of (5x1) reconstruction phase separation	0-0.6	300/1000	STM, LEED, ISS	[00Gil]
Cr/Au(100)	(1x1)	1.0		LEED	[94Hau]
Fe/Au(100)	(1x1)	1.0	300	HRLEED	[94Jia, 95Jia]
	Fe in subst. sites, place-exchange lifts "hex"-rec. and leads to Au islands	0-0.16	300	STM	[98Her]
Pb/Au(100)	c(2x2) $(7\sqrt{2}\times\sqrt{2})R45°$			LEED	[78Gre]

[a]) Ru(0001) substrate was generated by depositing thick Ru films onto a Mo(110) crystal.
[b]) Clear evidence for intermixing.
[c]) Surface alloy.
[e]) In islands reaching a critical diameter of 30 atoms one atomic row shifts by half a lattice constant onto bridge sites. This is the beginning of internal faceting continuing as strain relief mechanism up to 20 ML.
[f]) There is an abrupt structural transition to bct for $\theta > 1$ ML at 300 K $\leq T \leq$ 370 K, and for $\theta > 3$ ML at 370 K $\leq T \leq$ 420 K.

Acknowledgments
The author gratefully acknowledges help from S. Jans and C.-L. Bandelier in preparing the figures. He is also indebted to U. Heiz for carefully reading the manuscript.

Figures for 3.3.1

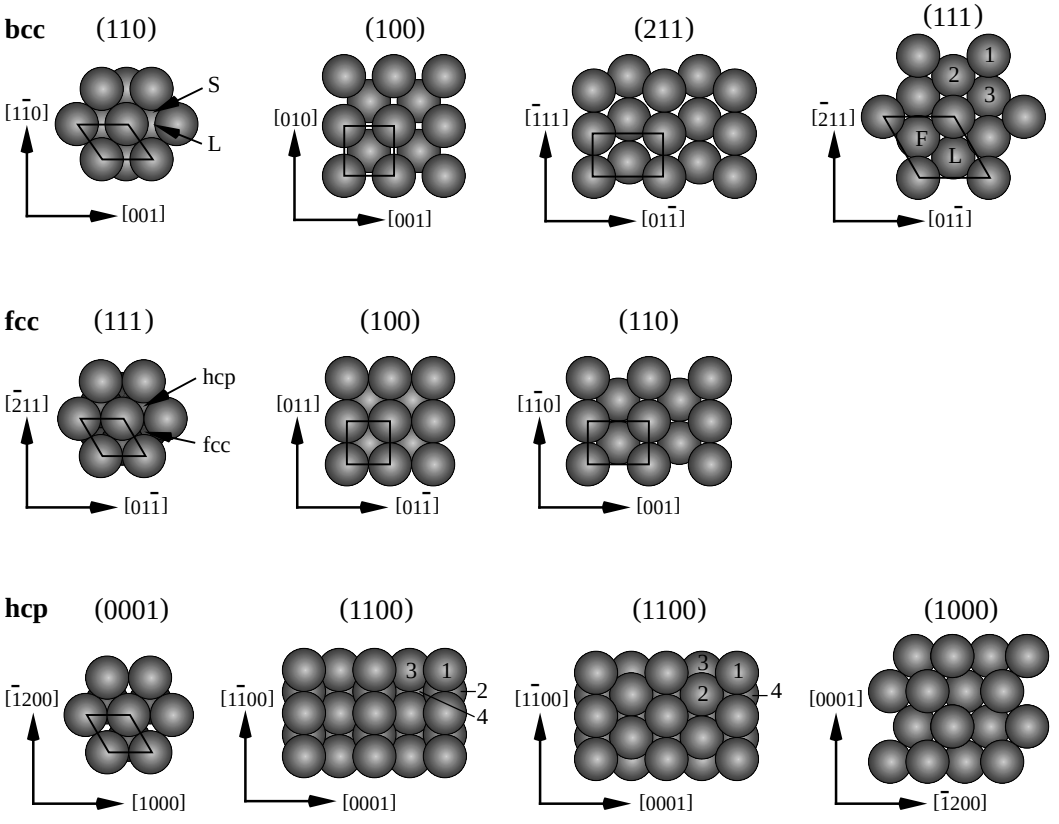

Fig. 1. The principal low-index surfaces of bcc, fcc and hcp crystals. For the hcp lattice the ideal packing with $c/a = 2\sqrt{6}/3$ is assumed. Two stacking sequences of the hcp(1100) plane are shown. In some cases the atoms are numbered according to the sequence of atomic planes. In the case of bcc(110) L stands for lattice and S for surface site; on the bcc(111) surface F labels the faulted site in contrast to the lattice continuation L; on fcc(111) the lattice site is labeled fcc and the faulted site hcp.

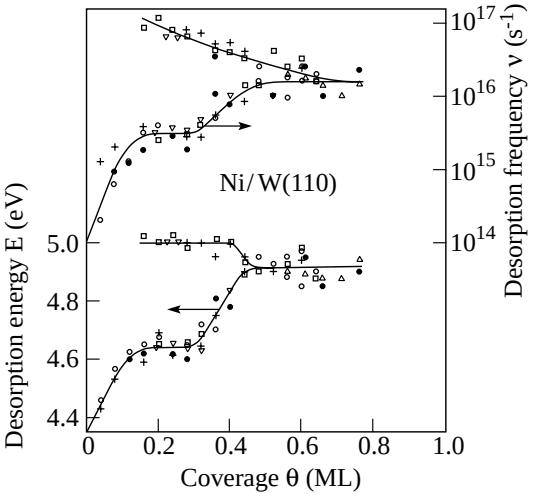

Fig. 2. Desorption energies $E_{des}(\theta)$ and pre-exponential factors $\nu_{des}(\theta)$ derived from TDS for Ni/W(110) [86Kol1]. Upper branches correspond to desorption from the 2D solid – gas interface, whereas lower branches are desorption from the 2D gas.

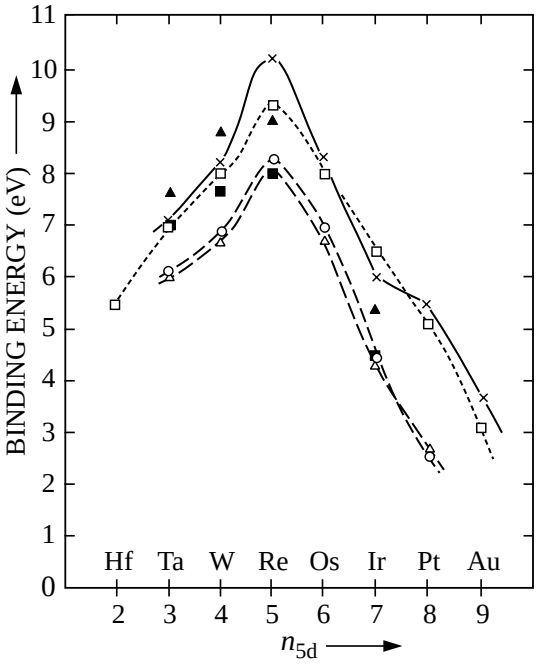

Fig. 3. Binding energies of 5d transition metal atoms on various W surfaces derived from critical voltages for field desorption. Crosses signify (110) surface orientation, squares (100), circles (112), and triangles (111); open and closed symbols indicate different evaluation procedures [84Bau1].

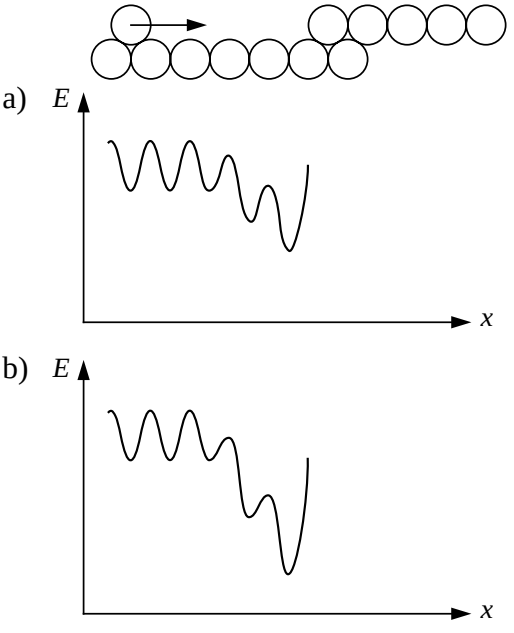

Fig. 4a, b. Attachment of an adatom to one- **(a)** and two- **(b)** fold step sites assuming attraction over two lattice sites. The energy barriers are drawn to scale for Ir/Ir(111).

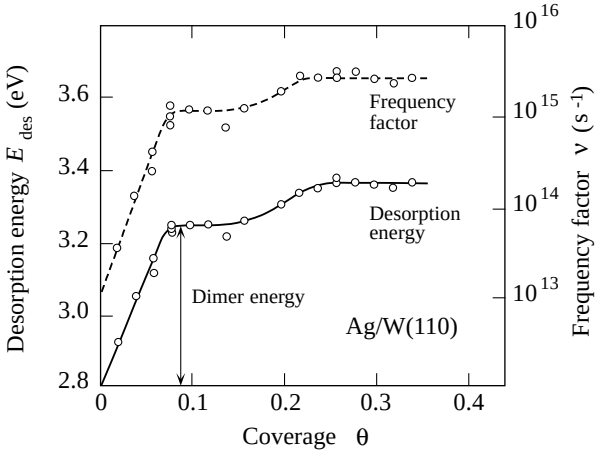

Fig. 5. Parameters for desorption from the 2D gas phase of Ag/W(110) [86Kol1].

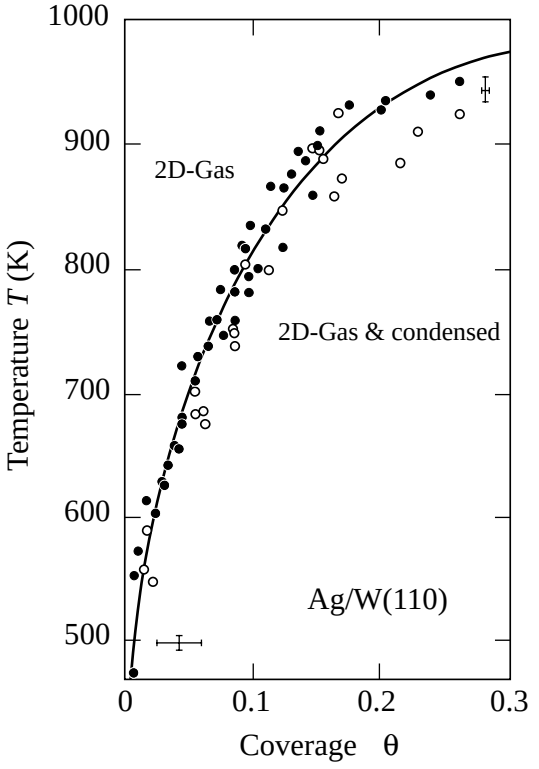

Fig. 6. Phase boundary separating pure lattice gas region from coexistence region of lattice gas and condensed phase in T-θ-diagram for Ag/W(110) [85Kol1].

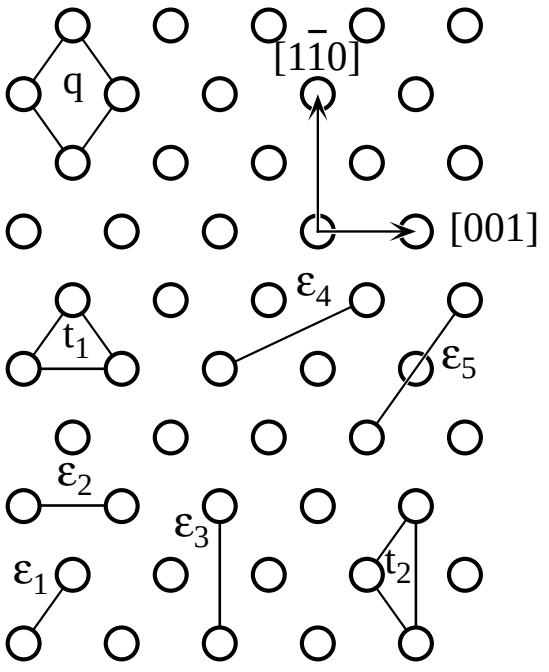

Fig. 7. Illustration of pair- and many-atom interac-tions contributing to binding in clusters on W(110) [89Roe].

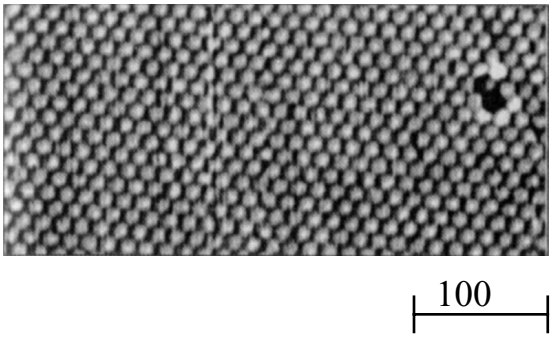

Fig. 8. STM image showing the pseudomorphic (1x1) monolayer of Cu on a Ru(0001) substrate [95Gün].

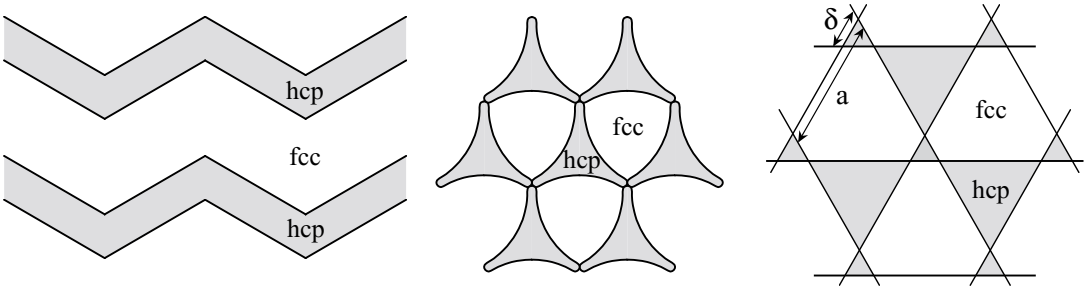

Fig. 9a - c. Possible domain wall structures for strain relief on hexagonally close packed surfaces: **(a)** unidirectional compression or expansion along the close packed atomic rows. For isotropic strain relief on a mesoscopic scale often two of the three possible rotational domains alternate leading to a herringbone pattern. **(b)** and **(c)** trigonal networks with wall crossings [97Bru].

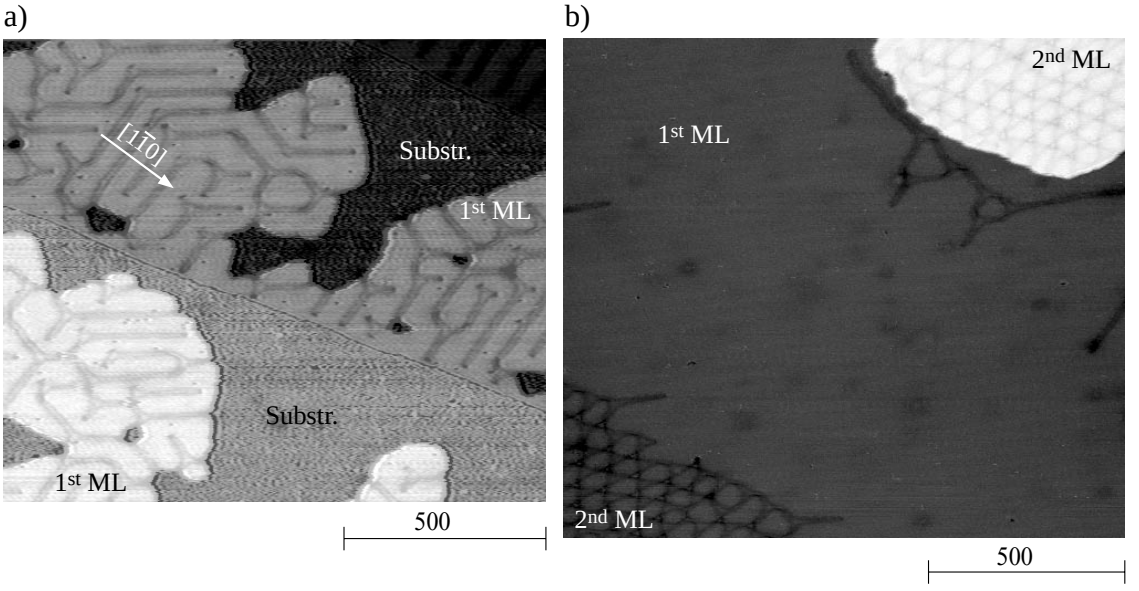

Fig. 10a, b. The first monolayer of Ag/Pt(111) forms **(a)** a pattern of partial surface dislocations for $\theta < 1.0$ ML and **(b)** a pseudomorphic layer as soon as 2. layer islands and thus a 2D Ag adatom gas are present on-top of the first layer (**(a)** θ = 0.5 ML, T_{dep} = 500 K, **(b)** θ = 1.5 ML, T_{dep} = 300 K, T_{ann} = 800 K) [97Bro].

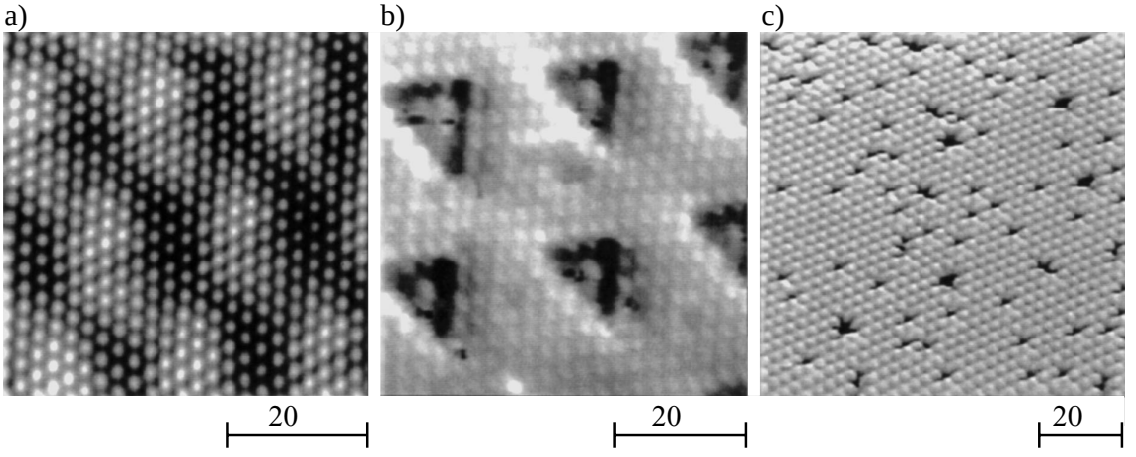

Fig. 11a - c. STM images of Ag deposited on Cu(111) showing the effect of substrate temperature during deposition. **(a)** Deposition of 0.8 ML at 225 K leads to a moiré pattern, while **(b)** deposition of the same amount at 300 K results in a triangular misfit dislocation structure. **(c)** Deposition of Ag submonolayers at 775 K leads to alloying of Ag atoms into the first Cu layer (dark spots) [97Bes].

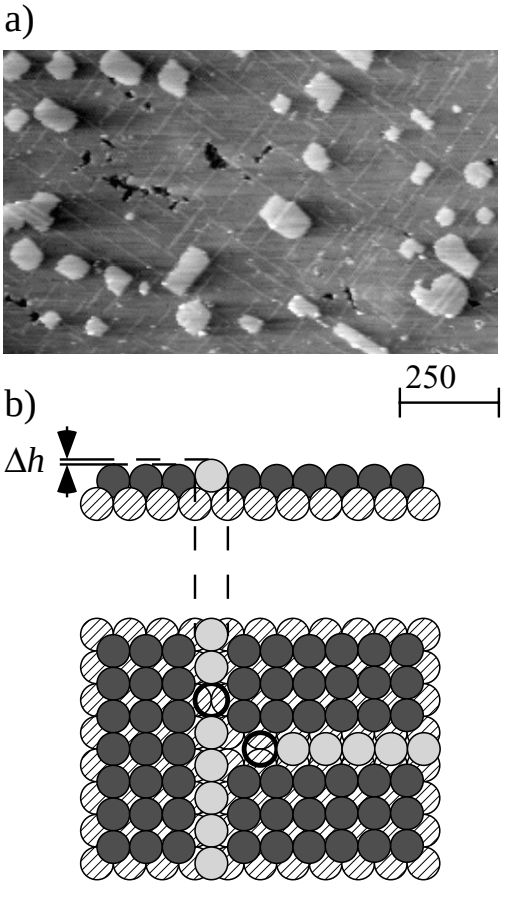

Fig. 12a, b. (a) Strain relief for a square lattice: Cu/Ni(100). **(b)** Single atomic Cu rows are shifted from 4-fold hollow to 2-fold bridge sites leading to the bright stripes in the STM image [96Mül2].

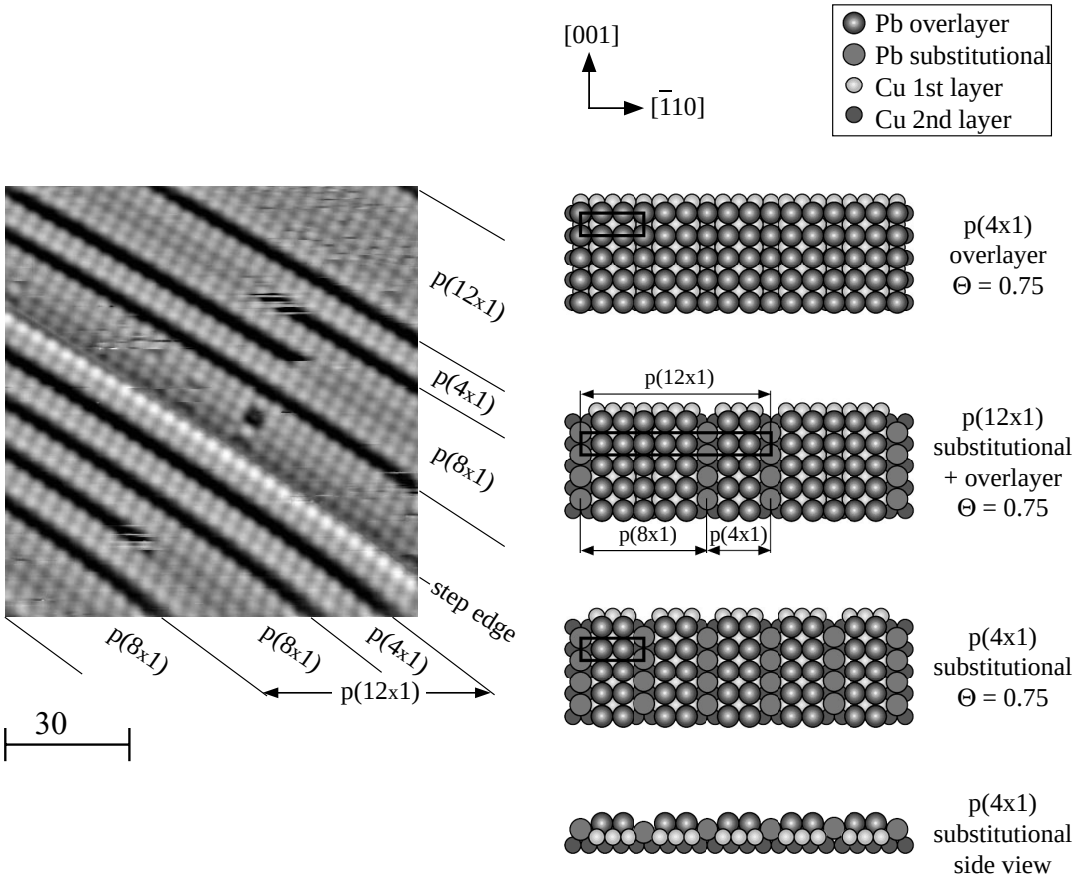

Fig. 13. STM image of 0.75 ML Pb on Cu(110). The superstructures depend critically on coverage. Upon a slight increase in θ (= Θ) the p(4x1) overlayer structure transforms into a structure with identical surface symmetry, but where one substrate [001]-row per unit-cell is substituted by a Pb row. Coexistence of ad- and substitutional structures lead to the p(12x1) and p(8x1) structures seen in the STM image. The substitutional rows lie lower and appear dark; the bright line is a step running across the image [95Nag1].

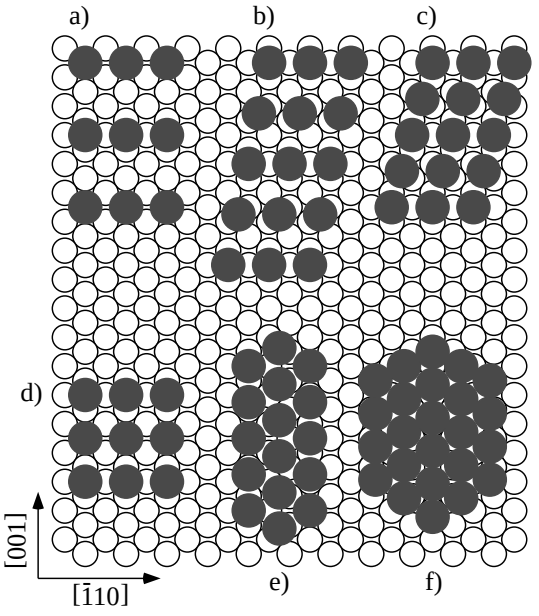

Fig. 14. Sequence of overlayer structures observed by means of LEED for Gd/W(110) with increasing coverage. (a) (10x2), (b) (7x2), (c) (5x2), (d) (6x2), (e) c(5x3), and (f) hexagonal for θ_s = 1/5, 2/7, 2/5, 1/3, 8/15, and 5/8, respectively [86Kol2].

References for 3.3.1

58Han Hansen, M.: "Constitution of Binary Alloys", New York, Toronto, London: Mc Graw Hill, 1958.
62Red Redhead, P.A.: Vacuum **12** (1962) 203.
64Ehr Ehrlich, G.: Brit. J. Appl. Phys. **15** (1964) 349.
65Gur Gurney, T., Hutchinson, F., Young, R.D.: J. Chem. Phys. **42** (1965) 3939.
65You Young, R.D., Schubert, D.S.: J. Chem. Phys. **42** (1965) 3943.
67Bau Bauer, E.: Surf. Sci. **7** (1967) 351.
67Jes Jesser, W.A., Matthews, J.M.: Philos. Mag. **15** (1967) 1097.
68Jes Jesser, W.A., Matthews, J.M.: Philos. Mag. **17** (1968) 595.
68Pal Palmberg, P.W., Rhodin, T.N.: J. Chem. Phys. **49** (1968) 134.
73Ven Venables, J.A.: Philos. Mag. **17** (1973) 697.
74Bau Bauer, E., Poppa, H., Todd, G., Bonczek, F.: J. Appl. Phys. **45** (1974) 5164.
74Gra Graham, W.R., Ehrlich, G.: Surf. Sci. **45** (1974) 530.
75Bas Bassett, D.W., Chung, C.K., Tice, D.: Vide **176** (1975) 39.
75Bau Bauer, E., Bonczek, F., Poppa, H., Todd, G.: Surf. Sci. **53** (1975) 87.
75Fal Falconer, J.L., Madix, R.J.: Surf. Sci. **48** (1975) 393.
75Kin King, D.A.: Surf. Sci. **47** (1975) 384.
76Gra Gradmann, U., Kümmerle, W., Tillmanns, P.: Thin Solid Films **34** (1976) 249.
76Syk1 Sykes, M.F., Gaunt, D.S., Glen, M.: J. Phys. A. Math. Gen. **9** (1976) 97.
76Syk2 Sykes, M.F., Glen, M.: J. Phys. A. Math. Gen. **9** (1976) 87.
77Erl Erlewein, J., Hofmann, S.: Surf. Sci. **68** (1977) 71.
77Fuj Fujinaga, Y.: Surf. Sci. **64** (1977) 751.
77Nov Novaco, A.D., McTague, J.P.: Phys. Rev. Lett. **38** (1977) 1286.
77Shi1 Shih, H.D., Jona, F., Jepsen, D.W., Marcus, P.M.: Phys. Rev. B **15** (1977) 5561.
77Shi2 Shih, H.D., Jona, F., Jepsen, D.W., Marcus, P.M.: Phys. Rev. B **15** (1977) 5550.
78Arg1 Argile, C., Rhead, G.E.: Surf. Sci. **78** (1978) 125.
78Arg2 Argile, C., Rhead, G.E.: Surf. Sci. **78** (1978) 115.
78Bib Biberian, J.P.: Surf. Sci. **74** (1978) 437.
78Ein Einstein, T.L.: CRC Crit. Rev. Sol. State Mater. Sci. **7** (1978) 261.
78Gre Green, A.K., Prigge, S., Bauer, E.: Thin Solid Films **52** (1978) 163.
78Jon Jones, R.G., Perry, D.L.: Surf. Sci. **71** (1978) 59.
78Lau Lau, K.H., Kohn, W.: Surf. Sci. **75** (1978) 69.
78Raw Rawlings, K.J., Gibson, M.J., Dobson, P.J.: J. Phys. D **11** (1978) 2059.
78Wea Weast, R.C.: (CRC Press, Cleveland, 78), p. D-62.
79Bak Bak, P., Mukamel, D., Villain, J., Wentowska, K.: Phys. Rev. B **19** (1979) 1610.
79Fuj Fujinaga, Y.: Surf. Sci. **84** (1979) 1.
79Jon Jones, R.G., Perry, D.L.: Surf. Sci. **82** (1979) 540.
79McT McTague, J.P., Novaco, A.D.: Phys. Rev. B **19** (1979) 5299.
80Arg Argile, C., Rhead, G.E.: Thin Solid Films **67** (1980) 299.
80Fin Fink, H.W., Faulian, K., Bauer, E.: Phys. Rev. Lett. **44** (1980) 1008.
80Fla Flahive, P.G., Graham, W.R.: Surf. Sci. **91** (1980) 463.
80Sch Schlenk, W., Bauer, E.: Surf. Sci. **93** (1980) 9.
80Wri Wrigley, J.D., Ehrlich, G.: Phys. Rev. Lett. **44** (1980) 661.
81Jon Jones, R.G., Perry, D.L.: Vacuum **31** (1981) 493.
81Tak Takayanagi, K.: Surf. Sci. **104** (1981) 527.
82Bau Bauer, E.: Appl. Surf. Sci. **11-12** (1982) 479.
82Com Comin, F., Citrin, P.H., Eisenberger, P., Rowe, J.E.: Phys. Rev. B **26** (1982) 7060.
82Dav Davies, P.W., Quinlan, M.A., Somorjai, G.A.: Surf. Sci. **121** (1982) 290.
82Smi Smith, G.C., Nooris, C., Binns, C., Padmore, H.A.: J. Phys. C **16** (1982) 1291.
82Tak Takayanagi, K.: Ultramicroscopy **8** (1982) 145.
82Tea Tear, S.P., Roell, K.: J. Phys. C **15** (1982) 5521.
82Voo Vook, R.W.: Internat. Metals Reviews **27** (1982) 209.
83Mir Miranda, R., Chandesris, D., Lecante, J.: Surf. Sci. **130** (1983) 269.

83Pes Pessa, M., Jylha, O.: Solid State Commun. **46** (1983) 419.
83Spi Spiller, G.D.T., Akhter, P., Venables, J.A.: Surf. Sci. **131** (1983) 517.
83Sto Stoop, L. C. A.: Thin Solid Films **103** (1983) 375.
83Tak Takayanagi, K., Yagi, K.: Trans. Jap. Inst. Met. **24** (1983) 337.
84Bau1 Bauer, E., in: "Chemisorption Systems, Part B", Vol. 3B, King, D.A., Woodruff, D.P. (eds.), Amsterdam: Elsevier Science, 1984, p. 1-57.
84Bau2 Bauer, E., Poppa, H.: Thin Solid Films **121** (1984) 159.
84Doe Doering, D.L., Semancik, S.: Phys. Rev. Lett. **53** (1984) 66.
84Fal Falo, F., Cano, I., Salmerón, M.: Surf. Sci. **143** (1984) 303.
84Hab Habenschaden, E., Küppers, J.: Surf. Sci. **138** (1984) L147.
84Kol Kolaczkiewicz, J., Bauer, E.: Phys. Rev. Lett. **53** (1984) 485.
84Rol Rolland, A., Bernardini, J.: Surf. Sci. **143** (1984) 579.
84Ven Venables, J.A., Spiller, G.D.T., Hanbücken, M.: Rep. Prog. Phys. **47** (1984) 399.
85Doe Doering, D.L.: J. Vac. Sci. Technol. A **3** (1985) 809.
85Har Harten, U., Lahee, A.M., Toennies, J.P., Wöll, C.: Phys. Rev. Lett. **54** (1985) 2619.
85Kol1 Kolaczkiewicz, J., Bauer, E.: Surf. Sci. **151** (1985) 333.
85Kol2 Kolaczkiewicz, J., Bauer, E.: Surf. Sci. **155** (1985) 700.
85Pri Prinz, G.A.: Phys. Rev. Lett. **54** (1985) 1051.
85Tak Takayanagi, K., Tanishiro, Y., Takahashi, M., Takahashi, S.: Surf. Sci. **164** (1985) 367.
85Yat Yates, J.T., Peden, C.H.F., Goodman, D.W.: J. Catal. **94** (1985) 576.
86Fin Fink, H.W.: IBM J. Res. Develop. **30** (1986) 460.
86Har Harendt, C., Christmann, K., Hirschwald, W., Vickerman, J.C.: Surf. Sci. **165** (1986) 413.
86Kol1 Kolaczkiewicz, J., Bauer, E.: Surf. Sci. **175** (1986) 487.
86Kol2 Kolaczkiewicz, J., Bauer, E.: Surf. Sci. **175** (1986) 508.
87Ash Ashcroft, N.W., Mermin, N.D.: "Solid State Physics", Philadelphia: HRW, 1987.
87Ber Berlowitz, P.J., Goodman, D.W.: Surf. Sci. **187** (1987) 463.
87Fei Feibelman, P.J.: Phys. Rev. Lett. **58** (1987) 2766.
87Jon Jones, R.G., Tong, A.W.L.: Surf. Sci. **188** (1987) 87.
87Kol Kolaczkiewicz, J.: Surf. Sci. **183** (1987) 251.
87Nie Niemantsverdriet, J.W., Dolle, P., Markert, K., Wandelt, K.: J. Vac. Sci. Technol. A **5** (1987) 875.
87One Onellion, M., Kime, Y.J., Dowben, P.A., Tache, N.: J. Phys. C **20** (1987) 1633.
87Par Park, C., Bauer, E., Poppa, H.: Surf. Sci. **187** (1987) 86.
87Ven Venables, J.A.: Phys. Rev. B **36** (1987) 4153.
87Wan Wang, Z.Q., Li, Y.S., Lok, C.K.C., Quinn, J., Jona, F., Marcus, P.M.: Solid State Commun. **62** (1987) 181.
88Ber1 Berlowitz, P.J., Goodman, D.W.: Langmuir **4** (1988) 1091.
88Ber2 Berlowitz, P.J., Houston, J.E., Wite, J.W., Goodman, D.W.: Surf. Sci. **205** (1988) 1.
88Lu Lu, S.H., Tian, D., Wang, Z.Q., Li, Y.S., Jona, F., Marcus, P.M.: Solid State Commun. **67** (1988) 325.
88Wu Wu, S.C., Lu, S.H., Wang, Z.Q., Lok, C.K.C., Quinn, J., Li, Y.S., Tian, D., Jona, F., Marcus, P.M.: Phys. Rev. B **38** (1988) 5363.
89Dov Dovek, M.M., Lang, C.A., Nogami, J., Quate, C.F.: Phys. Rev. B **40** (1989) 11973.
89Ege Egelhoff, W.F., Jacob, I.: Phys. Rev. Lett. **62** (1989) 921.
89Kla Klas, T., Fink, R., Krausch, S., Platzer, R., Voigt, J., Wesche, R., Schatz, G.: Surf. Sci. **216** (1989) 270.
89Roe Roelofs, L.D., Bellon, R.J.: Surf. Sci. **223** (1989) 585.
89Wan Wang, S.C., Ehrlich, G.: Phys. Rev. Lett. **62** (1989) 2297.
90Bar Barth, J.V., Brune, H., Ertl, G., Behm, R.J.: Phys. Rev. B **42** (1990) 9307.
90Ber Berlowitz, P.J., He, J.W., Goodman, D.W.: Surf. Sci. **231** (1990) 315.
90Bru Brune, H., Wintterlin, J., Ertl, G., Behm, R.J.: Europhys. Lett. **13** (1990) 123.
90Dow Dowben, P.A., Kime, Y.J., Hutchings, C.W., Li, W., Vidali, G.: Surf. Sci. **230** (1990) 113.
90Eva Evans, J.W., Sanders, D.E., Thiel, P.A., DePristo, A.E.: Phys. Rev. B **41** (1990) 5410.
90Fei Feibelman, P.J.: Phys. Rev. Lett. **65** (1990) 729.
90Fen Fenter, P., Gustafson, T.: Phys. Rev. Lett. **64** (1990) 1142.

90He He, J.W., Shea, W.L., Jiang, X., Goodman, D.W.: J. Vac. Sci. Technol. A **8** (1990) 2435.
90Koe Koel, B.E., Smith, R.J., Berlowitz, P.J.: Surf. Sci. **231** (1990) 325.
90Sin1 Singh, N.K., Jones, R.G.: Surf. Sci. **232** (1990) 243.
90Sin2 Singh, N.K., Jones, R.G.: Surf. Sci. **232** (1990) 229.
90Tia Tian, D., Lin, R.F., Jona, F.: Solid State Commun. **74** (1990) 1017.
90Tik Tikhov, M., Bauer, E.: Surf. Sci. **232** (1990) 73.
90Wan Wang, S.C., Ehrlich, G.: Surf. Sci. **239** (1990) 301.
91Att Attard, G.A., Bannister, A.: J. Electroanal. Chem. **300** (1991) 429.
91Bin Binns, C., Norris, C.: Condens. Mat. **3** (1991) 5425.
91Bor Borroni-Bird, C.E., Al-Sarraf, N., Andersson, S., King, D.A.: Chem. Phys. Lett. **183** (1991) 516.
91Bro Brodde, A., Wilhelmi, G., Badt, D., Wengelnik, H., Neddermeyer, H.: J. Vac. Sci. Technol. B **9** (1991) 920.
91Cha1 Chambliss, D.D., Wilson, R.J.: J. Vac. Sci. Technol. B **9** (1991) 928.
91Cha2 Chambliss, D.D., Wilson, R.J., Chiang, S.: Phys. Rev. Lett. **66** (1991) 1721.
91Che Chen, C., Tsong, T.T.: Phys. Rev. Lett. **66** (1991) 1610.
91Ehr Ehrlich, G., Watanabe, F.: Langmuir **7** (1991) 2555.
91Fen Fenter, P., Gustafsson, T.: Phys. Rev. B **43** (1991) 12195.
91Jia Jiang, X., Goodman, D.W.: Surf. Sci. **255** (1991) 1.
91Kel Kellogg, G.L.: Phys. Rev. Lett. **67** (1991) 216.
91Pöt Pötschke, G.O., Behm, R.J.: Phys. Rev. B **44** (1991) 1442.
91San Sanders, D.E., DePristo, A.E.: Surf. Sci. **254** (1991) 341.
91San Sandy, A.R., Mochrie, S.G.J., Zehner, D.M., Huang, K.G., Gibbs, D.: Phys. Rev. B **43** (1991) 4667.
91Voi1 Voigtländer, B., Meyer, G., Amer, N.M.: Phys. Rev. B **44** (1991) 10354.
91Voi2 Voigtländer, B., Meyer, G., Amer, N.M.: Surf. Sci. **255** (1991) L529.
91Wan Wang, S.C., Ehrlich, G.: J. Chem. Phys. **94** (1991) 4071.
91Wat Watanabe, F., Ehrlich, G.: J. Chem. Phys. **95** (1991) 6075.
92Bro Brodde, A., Neddermeyer, H.: Ultramicroscopy **42-44** (1992) 556.
92Cam Campbell, R.A., Rodriguez, J.A., Goodman, D.W.: Phys. Rev. B **46** (1992) 7077.
92Cha1 Chambliss, D.D., Chiang, S.: Surf. Sci. **264** (1992) L187.
92Cha2 Chambliss, D.D., Wilson, R.J., Chiang, S.: J. Vac. Sci. Technol. A **10** (1992) 1993.
92Che Chen, C., Tsong, T.T.: Phys. Rev. B **46** (1992) 7803.
92Hwa Hwang, R.Q., Behm, R.J.: J. Vac. Sci. Technol. B **10** (1992) 256.
92Kim Kime, Y.J., Jiandi, Z., Dowben, P.A.: Surf. Sci. **268** (1992) 98.
92Koe Koel, B.E., Sellidj, A., Paffett, M.T.: Phys. Rev. B **46** (1992) 7846.
92McM McMahon, E., Horschorn, E.S., Chiang, T.C.: Surf. Sci. **279** (1992) L231.
92Nar Narasimhan, S., Vanderbilt, D.: Phys. Rev. Lett. **69** (1992) 1564.
92Rod1 Rodriguez, J.A., Champbell, R.A., Goodman, D.W.: J. Vac. Sci. Technol. A **10** (1992) 2540.
92Rod2 Rodriguez, J.A., Hrbek, J.: J. Chem. Phys. **97** (1992) 9427.
92Rou Rousset, S., Chiang, S., Fowler, D.E., Chambliss, D.D.: Phys. Rev. Lett. **69** (1992) 3200.
92Sch Schröder, J., Günther, C., Hwang, R.Q., Behm, R.J.: Ultramicr. **42-44** (1992) 475.
92Str Stroscio, J.A., Pierce, D.T., Dragoset, R.A., First, P.N.: J. Vac. Sci. Technol. A **10** (1992) 1981.
92Wat Watanabe, F., Ehrlich, G.: J. Chem. Phys. **96** (1992) 3191.
93Beg Begley, A.M., Tian, D., Jona, F., Marcus, P.M.: Surf. Sci. **280** (1993) 289.
93Bot Bott, M., Hohage, M., Michely, T., Comsa, G.: Phys. Rev. Lett. **70** (1993) 1489.
93Cha Chambliss, D.D., Johnson, K.E., Wilson, R.J., Chiang, S.: J. Magn. Magn. Mater. **121** (1993) 1.
93Eis Eisenhut, B., Stober, J., Rangelov, G., Fauster, T.: Phys. Rev. B **47** (1993) 12980.
93Fig Figuera, J. d. l., Prieto, J.E., Ocal, C., Miranda, R.: Phys. Rev. B **47** (1993) 13043.
93Fis Fischer, A., Fasel, R., Osterwalder, J., Krozer, A., Schlappbach, L.: Phys. Rev. Lett. **70** (1993) 1493.
93Joh Johnson, K.E., Chambliss, D.D., Wilson, R.J., Chiang, S.: J. Vac. Sci. Technol. A **11** (1993) 1654.
93Li Li, W., Vidali, G., Biham, O.: Phys. Rev. B **48** (1993) 8336.
93Nak Nakanishi, S., Kawamoto, K., Umezawa, K.: Surf. Sci. **287-288** (1993) 974.
93Nau Naumovic, D., Osterwalder, J., Stuck, A., Aebi, P., Schlapbach, L.: Surf. Sci. **287-288** (1993) 950.

93Nie Nielsen, L.P., Besenbacher, F., Lægsgaard, E., Stensgaard, I., Engdahl, C., Stoltze, P., Jacobsen, K.W., Nørskov, J.K.: Phys. Rev. Lett. **71** (1993) 754.
93Nyb Nyberg, G.L., Kief, M. T., Egelhoff, W.F.: Phys. Rev. B **48** (1993) 14509.
93Röd Röder, H., Schuster, R., Brune, H., Kern, K.: Phys. Rev. Lett. **71** (1993) 2086.
93Rod Rodriguez, J.A.: Surf. Sci. **296** (1993) 149.
93Str Strüber, U., Küppers, J.: Surf. Sci. **294** (1993) L924.
93Stu Stuckless, J.T., Al-Sarraf, N., Wartnaby, C., King, D.A.: J. Chem. Phys. **99** (1993) 2202.
93Tob Tobin, J.G., Waddill, G.D., Li, H., Tong, S.V.: Phys. Rev. Lett. **70** (1993) 4150.
93Vri Vrijmoeth, J., Günther, C., Schröder, J., Hwang, R.Q., Behm, R.J., in: "Magnetism, Structure in Systems of Reduced Dimension", Farrow, R.F.C. (ed.), New York: Plenum Press, 1993, p. 55.
93Wan1 Wang, S.C., Ehrlich, G.: Phys. Rev. Lett. **70** (1993) 41.
93Wan2 Wang, S.C., Ehrlich, G.: Phys. Rev. Lett. **71** (1993) 4174.
93Wut1 Wuttig, M., Flores, T., Knight, C.C.: Phys. Rev. B **48** (1993) 12082.
93Wut2 Wuttig, M., Gauthier, Y., Blügel, S.: Phys. Rev. Lett. **70** (1993) 3619.
93Zha Zhang, J., Han, Z. L., Varma, S.: Surf. Sci. **298** (1993) 351.
94Alt Altman, E.I., Colton, R.J.: Surf. Sci. **304** (1994) L400.
94Att Attard, G.A., Price, R., Al-Akl, A.: Electrochim. Acta **38** (1994) 1525.
94Bru Brune, H., Röder, H., Boragno, C., Kern, K.: Phys. Rev. B **49** (1994) 2997.
94Buc Bucher, J.P., Hahn, E., Fernandez, P., Massobrio, C., Kern, K.: Europhys. Lett. **27** (1994) 473.
94Cha Chambliss, D.D., Johnson, K.E.: Phys. Rev. B **50** (1994) 5012.
94Eis Eisenhut, B., Stober, J., Rangelov, G., Fauster, T.: Phys. Rev. B **49** (1994) 12980.
94Fei1 Feibelman, P.J.: Surf. Sci. **313** (1994) L801.
94Fei2 Feibelman, P.J., Nelson, J.S., Kellogg, G.L.: Phys. Rev. B **49** (1994) 10548.
94Grü Grütter, P., Dürig, U.T.: Phys. Rev. B **49** (1994) 2021.
94Hah Hahn, E., Kampshoff, E., Fricke, A., Bucher, J.P., Kern, K.: Surf. Sci. **319** (1994) 277.
94Hau Haugan, M.E., Qibiao, C., Onellion, M., Himpsel, F.J.: Phys. Rev. B **49** (1994) 14028.
94Jia Jiang, Q., Chan, A., Wang, G.C.: Phys. Rev. B **50** (1994) 11116.
94Kel Kellogg, G.L.: Surf. Sci. Rep. **21** (1994) 1.
94Nag Nagl, C., Haller, O., Platzgummer, E., Schmid, M., Varga, P.: Surf. Sci. **321** (1994) 237.
94Rab Rabe, A., Memmel, N., Steltenpohl, A., Fauster, T.: Phys. Rev. Lett. **73** (1994) 2728.
94Som Somorjai, G.A.: "Introduction to Surface Chemistry and Catalysis", New York: John Wiley & Sons, 1994.
94Van Vandoni, G., Félix, C., Monot, R., Buttet, J., Harbich, W.: Surf. Sci. **320** (1994) L63.
95Atr Atrei, A., Bardi, U., Galeotti, M., Rovida, G., Torrini, M.,anazzi, E.: Surf. Sci. **339** (1995) 323.
95Boi Boisvert, G., Lewis, L.J., Puska, M.J., Nieminen, R.M.: Phys. Rev. B **52** (1995) 9078.
95Dor Dorenbos, G., Boerma, D.O., Buck, T.M., Wheatley, G.H.: Phys. Rev. B **51** (1995) 4485.
95Fri Fritzsche, H., Meyer, G., Amer, N.M.: Phys. Rev. B **51** (1995) 15933.
95Grü Grütter, P., Dürig, U.: Surf. Sci. **337** (1995) 147.
95Gua Guan, J., Campbell, R.A., Madey, T.E.: Surf. Sci. **341** (1995) 311.
95Gün Günther, C., Vrijmoeth, J., Hwang, R.Q., Behm, R.J.: Phys. Rev. Lett. **74** (1995) 754.
95Hah Hahn, E., Kampshoff, E., Wälchli, N., Kern, K.: Phys. Rev. Lett. **74** (1995) 1803.
95Hwa Hwang, R.Q., Hamilton, J.C., Stevens, J.L., Foiles, S.M.: Phys. Rev. Lett. **75** (1995) 4242.
95Jac Jacobsen, J., Nielsen, L.P., Besenbacher, F., Stensgaard, I., Lægsgaard, E., Rasmussen, T., Jacobsen, K.W., Nørskov, J.K.: Phys. Rev. Lett. **75** (1995) 489.
95Jia Jiang, Q., Wang, G.C.: Surf. Sci. **324** (1995) 357.
95Mey1 Meyer, J.A., Behm, R.J.: Surf. Sci. **322** (1995) L275.
95Mey2 Meyer, J.A., Schmid, P., Behm, R.J.: Phys. Rev. Lett. **74** (1995) 3864.
95Nag1 Nagl, C., Pinczolits, M., Schmid, M., Varga, P., Robinson, I.K.: Phys. Rev. B **52** (1995) 16796.
95Nag2 Nagl, C., Platzgummer, E., Schmid, M., Varga, P., Speller, S., Heiland, W.: Phys. Rev. Lett. **75** (1995) 2976.
95Nie Nielsen, L.P., Besenbacher, F., Stensgaard, I., Lægsgaard, E., Engdahl, C., Stoltze, P., Nørskov, J.K.: Phys. Rev. Lett. **74** (1995) 1159.
95Pou Poulston, S., Tikhov, M., Lambert, R.M.: Surf. Sci. **331-333** (1995) 818.
95Ste Stevens, J.L., Hwang, R.Q.: Phys. Rev. Lett. **74** (1995) 2078.

95Tob Tobin, J.G., Waddill, G.D., Hua, L., Tong, S.Y.: Surf. Sci. **334** (1995) 263.
95Wu Wu, Y., Tao, H.S., Garfunkel, E., Madey, T.E., Shinn, N.D.: Surf. Sci. **336** (1995) 123.
96Dav Davies, A., Stroscio, J.A., Pierce, D.T., Celotta, R.J.: Phys. Rev. Lett. **76** (1996) 4175.
96Fig Figuera, J. d. a., Prieto, J.E., Kostka, G., Müller, S., Ocal, C., Miranda, R., Heinz, K.: Surf. Sci. **349** (1996) L139.
96Göl Gölzhäuser, A., Ehrlich, G.: Phys. Rev. Lett. **77** (1996) 1334.
96Hol Holmblad, P.M., Larsen, J.H., Chorkendorff, I., *et al.*: Catalysis Letters **40** (1996) 131.
96Hug Hugenschmidt, M.B., Hitzke, A., Behm, R.J.: Phys. Rev. Lett. **76** (1996) 2535.
96Kel Kellogg, G.L.: Phys. Rev. Lett. **76** (1996) 98.
96Kop Kopatzki, E., Keck, H.G., Baikie, I.D., Meyer, J.A., Behm, R.J.: Surf. Sci. **345** (1996) L11.
96Law Lawler, J.F., Kraan, R.G.P. v. d., Kempen, H. v., Quinn, A.J.: Phys. Rev. B **53** (1996) 11159.
96Mey Meyer, J.A., Baikie, J.D., Kopatzki, E., Behm, R.J.: Surf. Sci. **365** (1996) L647.
96Mül1 Müller, B., Fischer, B., Nedelmann, L., Brune, H., Kern, K.: Phys. Rev. B **54** (1996) 17858.
96Mül2 Müller, B., Fischer, B., Nedelmann, L., Fricke, A., Kern, K.: Phys. Rev. Lett. **76** (1996) 2358.
96Mur Murray, P.W., Stensgaard, I., Lægsgaard, E., Besenbacher, F.: Surf. Sci. **365** (1996) 591.
96Nag Nagl, C., Schmid, M., Varga, P.: Surf. Sci. **369** (1996) 159.
96Nor Noro, H., Persaud, R., Venables, J.A.: Surf. Sci. **357-358** (1996) 879.
96Pat Patthey, F., Massobrio, C., Schneider, W.D.: Phys. Rev. 53 **53** (1996) 13146.
96Sch1 Schneider, W.D., Patthey, F., Roy, H.V., Schaffner, M.H., Delley, B.: Mod. Phys. Lett. B **10** (1996) 1161.
96Sch2 Schwegmann, S., Over, H., Gierer, M., Ertl, G.: Phys. Rev. B **53** (1996) 11164.
96She1 Shen, Y.G., Yao, J., O'Connor, D.J., King, B.V., MacDonald, R.J.: J. Phys. Cond. Mat. **8** (1996) 4903.
96She2 Shen, Y.G., Yao, J., O'Connor, D.J., King, B.V., MacDonald, R.J.: Solid State Commun. **100** (1996) 21.
96Spr Sprunger, P.T., Lægshaard, E., Besenbacher, F.: Phys. Rev. B **54** (1996) 8163.
96Stu Stuck, A., Wartnaby, C.E., Yeo, Y.Y., Stuckless, J.T., Al-Sarraf, N., King, D.A.: Surf. Sci. **249** (1996) 229.
96Stu Stumpf, R., Scheffler, M.: Phys. Rev. B **53** (1996) 4958.
96Tan Tanaka, Y., Kamei, M., Gotoh, Y.: Surf. Sci. **360** (1996) 74.
96Yeo Yeo, Y.Y., Vattuone, L., King, D.A.: J. Chem. Phys. **104** (1996) 3810.
97Bes Besenbacher, F., Nielsen, L.P., Sprunger, P.T., in: "Growth and Properties of Ultrathin Epitaxial Layers", Vol. 8, King, D.A., Woodruff, D.P. (eds.), Amsterdam: Elsevier, 1997, p. 207.
97Bro Bromann, K., Brune, H., Giovannini, M., Kern, K.: Surf. Sci. **388** (1997) L1107.
97Cha Champbell, C.T.: Surf. Sci. Rep. **27** (1997) 1.
97Chr Christensen, A., Ruban, A.V., Stoltze, P., Jacobsen, K.W., Skriver, H.L., Nørskov, J.K., Besenbacher, F.: Phys. Rev. B **56** (1997) 5822.
97Fer Ferrer, S., Alvarez, J., Lundgren, E., Torrelles, X., Fajardo, P., Boscherini, F.: Phys. Rev. B **56** (1997) 9848.
97Fis Fischer, B., Barth, J.V., Fricke, A., Nedelmann, L., Kern, K.: Surf. Sci. **389** (1997) 366.
97Gle Gleich, B., Ruff, M., Behm, R.J.: Surf. Sci. **386** (1997) 488.
97Gün Günther, S., Hitzke, A., Behm, R.J.: Surf. Rev., Lett. **4** (1997) 1103.
97Hit Hitzke, A., Hugenschmidt, M.B., Behm, R.J.: Surf. Sci. **389** (1997) 8.
97Hol Holst, B., Hohlen, M., Wandelt, K., Allison, W.: Surf. Sci. **377-379** (1997) 891.
97Hug Hugenschmidt, M.B., Ruff, M., Hitzke, A., Behm, R.J.: Surf. Sci. **388** (1997) L1100.
97Kin King, D.A., Woodruff, D.P., in: The Chemical Physics of Solid Surfaces, Vol. 8. Amsterdam: Elsevier Science, 1997.
97Lan Langelaar, M.H., Boerma, D.O., in: "Surface Diffusion: Atomistic and Collective Processes", Vol. 360, Tringides, M.C. (ed.), New York: Plenum Press, 1997, p. 67.
97Li Li, Y., Bartelt, M.C., Evans, J.W., Waelchli, N., Kampshoff, E., Kern, K., DePristo, A.E.: Phys. Rev. B **56** (1997) 12539.
97Lin Linderoth, T.R., Horch, S., Lægsgaard, E., Stensgaard, I., Besenbacher, F.: Phys. Rev. Lett. **78** (1997) 4978.

97Mur Murray, P.W., Thorshaug, S., Stensgaard, I., Besenbacher, F., Lægsgaard, E., Ruban, A.V., Jacobsen, K.W., Kopidakis, G., Skriver, H.L.: Phys. Rev. B **55** (1997) 1380.
97Par Parschau, M., Schlatterbeck, D., Christmann, K.: Surf. Sci. **376** (1997) 133.
97Pas Pascal, R., Zarnitz, C., Bode, M., Wiesendanger, R.: Phys. Rev. B **56** (1997) 3636.
97Ped Pedersen, M.Ø., Bönicke, I.A., Lægsgaard, E., Stensgaard, I., Ruban, A., Nørskov, J.K., Besenbacher, F.: Surf. Sci. **387** (1997) 86.
97Pfa Pfandzelter, R., Igel, T., Winter, H.: Surf. Sci. **389** (1997) 317.
97Töl1 Tölkes, C., Zeppenfeld, P., Krzyzowski, M.A., David, R., Comsa, G.: Phys. Rev. B **55** (1997) 13932.
97Töl2 Tölkes, C., Zeppenfeld, P., Krzyzowski, M.A., David, R., Comsa, G.: Surf. Sci. **394** (1997) 170.
97Yeo1 Yeo, Y.Y., Vattuone, L., King, D.A.: J. Chem. Phys. **106** (1997) 392.
97Yeo2 Yeo, Y.Y., Vattuone, L., King, D.A.: J. Chem. Phys. **106** (1997) 1990.
98Bes Besenbacher, F., Chorkendorff, I., Clausen, B.S., Hammer, B., Molenbroek, A.M., Nørskov, J.K., Stensgaard, I.: Science **279** (1998) 1913.
98Boc Bocquet, F., Gauthier, S.: Surf. Sci. **416** (1998) 1.
98Bro Brown, W.., Kose, R., King, D.A.: Chem. Reviews **98** (1998) 797.
98Bru Brune, H.: Surf. Sci. Rep. **31** (1998) 121.
98Cho Choi, B.C., Bode, P.J., Bland, J.A.C.: Phys. Rev. B **58** (1998) 5166.
98Gor Gorodetsky, D.A., Melnik, Y.P., Proskurin, D.P., Sklyar, V.K., Usenko, V.A.,, Yas'ko, A.A.: Surf. Sci. **416** (1998) 255.
98Hah Hahn, P., Bertino, M.F., Toennies, J.P., Ritter, M., Weiss, W.: Surf. Sci. **412-413** (1998) 82.
98Her Hernán, O.S., Parga, A.L.V. a. d., Gallego, J.M., Miranda, R.: Surf. Sci. **415** (1998) 106.
98Hir Hirstein, A.: Ph.D.-Thesis, Lausanne: Ecole Polytechnique Fédérale, 1998.
98Hol Holst, B., Nohlen, M., Wandelt, K., Allison, W.: Phys. Rev. B **58** (1998) R10195.
98Kyu Kyuno, K., Gölzhäser, A., Ehrlich, G.: Surf. Sci. **397** (1998) 191.
98Mon Mongeot, F.B. d., Scherer, M., Gleich, B., Kopatzki, E., Behm, R.J.: Surf. Sci. **411** (1998) 249.
98Pim Pimpinelli, A., Villain, J.: "Physics of Crystal Growth", Cambridge: Cambridge University Press, 1998.
98Pla Platzgummer, E., Borell, M., Nagl, C., Schmid, M., Varga, P.: Surf. Sci. **412-413** (1998) 202.
98Sam Sambi, M., Granozzi, G.: Surf. Sci. **400** (1998) 239.
98Sch Schlatterbeck, P., Parschau, M., Christmann, K.: Surf. Sci. **418** (1998) 240.
98Ste Stepanowskyi, S., Ubogy, I., Kolaczkiewicz, J.: Surf. Sci. **411** (1998) 176.
98Töl Tölkes, C., Struck, R., David, R., Zeppenfeld, P., Comsa, G.: Phys. Rev. Lett. **80** (1998) 2877.
98Tsa Tsay, J.S., Shern, C.S.: Surf. Sci. **396** (1998) 319.
98Veg Vegt, H.A. v. d., Vrijmoeth, J., Behm, R.J., Vlieg, E.: Phys. Rev. B **57** (1998) 4127.
98Wah Wahlström, E., Ekvall, I., Olin, H., Walldén, L.: Appl. Phys. A **66** (1998) S1107.

98Zha Zhang, Z., Lagally, M.G., in: Series in Direction in Condensed Matter Physics, Vol. 14, Singapore: World Scientific, 1998.
99Bod Bode, M., Hennefarth, M., Haude, D., Getzlaff, M., Wiesendanger, R.: Surf. Sci. **432** (1999) 8.
99Bro Brown, D., Noakes, T.C.Q., Woodruff, D.P., Bailey, P., Le-Goaziou, Y.: J. Phys. Cond. Mat. **11** (1999) 1889.
99Bru Brune, H., Bales, G.S., Boragno, C., Jacobsen, J., Kern, K.: Phys. Rev. B **60** (1999) 5991.
99Cho1 Choi, B.C., Bode, P.J., Bland, J.A.C.: Phys. Rev. B **59** (1999) 7029.
99Cho2 Choi, Y.J., Jeong, I.C., Park, J.-Y., Kahng, S.-J., Lee, J., Kuk, Y.: Phys. Rev. B **59** (1999) 10918.
99Fei Feibelman, P.: Phys. Rev. B **60** (1999) 4972.
99Fis Fischer, B., Brune, H., Fricke, A., Barth, J.V., Kern, K.: Phys. Rev. Lett. **82** (1999) 1732.
99Hen Henzler, M.: Surf. Sci. **419** (1999) 321.
99Hua Huang, H.H., Jiang, X., Siew, H.L., Chin, W.S., Sim, W.S., Xu, G.Q.: Surf. Sci. **436** (1999) 167.
99Jea Jeandupeux, O., Bürgi, L., Hirstein, A., Brune, H., Kern, K.: Phys. Rev. B **59** (1999) 15926.
99Jo1 Jo, S., Gotoh, Y.: Jap. J. Appl. Phys. **38** (1999) 6878.
99Jo2 Jo, S., Gotoh, Y.: Surf. Sci. **435** (1999) 652.
99Kah Kahng, S.J., Park, J.V., Kuk, Y.: Surf. Sci. **442** (1999) 379.
99Koh Koh, S.J., Ehrlich, G.: Phys. Rev. B **60** (1999) 5981.

99Kol1 Kolaczkiewicz, J., Bauer, E.: Surf. Sci. **420** (1999) 157.
99Kol2 Kolaczkiewicz, J., Bauer, E.: Surf. Sci. **423** (1999) 292.
99Kra Kralj, M., Pervan, P., Milun, M.: Surf. Sci. **423** (1999) 24.
99Kyu Kyuno, K., Ehrlich, G.: Surf. Sci. **437** (1999) 29.
99Luc Luches, P., Gazzadi, G.C., Bona, A. d., Marassi, L., Pasquali, L., Valeri, S., Nannarone, S.: Surf. Sci. **419** (1999) 207.
99Lun1 Lundgren, E., Stanka, B., Koprolin, W., Schmid, M., Varga, P.: Surf. Sci. **423** (1999) 357.
99Lun2 Lundgren, E., Stanka, B., Leonardelli, G., Schmid, M., Varga, P.: Phys. Rev. Lett. **82** (1999) 5068.
99Nou Nouvertné, F., May, U., Bamming, M., Rampe, A., Korte, U., Güntherodt, G., Pentcheva, R., Scheffler, M.: Phys. Rev. B **61** (1999) 14382.
99Pad Padovani, S., Scheurer, F., Bucher, J. P.: Euophys. Lett. **45** (1999) 327.
99Par Parschau, M., Christmann, K.: Surf. Sci. **423** (1999) 303.
99Ped Pedersen, M. Ø., Helveg, S., Ruban, A., Stensgaard, I., Lægsgaard, E., Nørskov, J. K., Besenbacher, F.: Surf. Sci. **426** (1999) 395.
99Pel Pelhos, K., Hannon, J.B., Kellogg, G.L., Madey, T.E.: Surf. Sci. **432** (1999) 115.
99Ram Ramstad, A., Strisland, F., Raaen, S., Worren, T., Borg, A., Berg, C.: Surf. Sci. **425** (1999) 57.
99Sam Sambi, N., Granozzi, G.: Surf. Sci. **426** (1999) 235.
99Sch Schieffer, P., Tuillier, M.H., Hanf, M.C., Krembel, C., G, G.: Surf. Sci. **422** (1999) 132.
99Sha Shakirova, S.A., Serova, E.V.: Surf. Sci. **422** (1999) 24.
99Ter Terada, S., Yokoyama, T., Saito, N., Okamoto, Y., Ohta, T.: Surf. Sci. **433-435** (1999) 657.
99Tod Todorov, S.S., Bu, H., Boyd, K.J., Rabalais, J.W., Gilmore, C.M., Sprague, J.A.: Surf. Sci. **429** (1999) 63.
99Töl Tölkes, C., David, R., Tscherisch, K.G., Comsa, G., Zeppenfeld, P.: Europhys. Lett. **46** (1999) 589.
99Tsu Tsunematsu, H., Aita, M., Tanaka, A., Suzuki, S., Sato, S., Gotoh, Y.: J. El. Spectr. & Rel. Phen. **103** (1999) 281.
99Wag Wagner, R., Schlatterbeck, D., Christmann, K.: Surf. Sci. **440** (1999) 231.
00Bar Barth, J.V., Brune, H., Fischer, B., Weckesser, J., Kern, K.: Phys. Rev. Lett. **84** (2000) 1732.
00Ber Bertacco, R., Isella, G., Duò, L., Ciccacci, F., Bona, A. d., Luches, P., Valeri, S.: Surf. Sci. **454-456** (2000) 671.
00Bog Bogicevic, A., Ovesson, S., Hyldgaard, P., Lundqvist, B.I., Brune, H., Jennison, D.R.: Phys. Rev. Lett. **85** (2000) 1910.
00But Butterfield, M.T., Crapper, M.D.: Surf. Sci. **454-456** (2000) 719.
00Cab Cabeza, G.F., Légaré, P., Sadki, A., Castellani, N.J.: Surf. Sci. **457** (2000) 121.
00D'Ad D'Addato, S., Pasquali, L., Gazzadi, G.C., Verucchi, R., Capelli, R., Nannarone, S.: Surf. Sci. **454-456** (2000) 692.
00Deg Degroote, B., Dekoster, J., Langouche, G.: Surf. Sci. **452** (2000) 172.
00Fey Feydt, J., Elbe, A., Meister, G., Goldmann, A.: Surf. Sci. **445** (2000) 115.
00Fic Fichthorn, K. A., Scheffler, M.: Phys. Rev. Lett. **84** (2000) 5371.
00Gil Gilarowski, G., Méndez, J., Niehus, H.: Surf. Sci. **448** (2000) 290.
00Hel Helveg, S., Lauritsen, J.V., Lægsgaard, E., Stensgaard, I., Nørkov, J.K., Clausen, B.S., Topsøe, H., Besenbacher, F.: Phys. Rev. Lett. **84** (2000) 951.
00Hyl Hyldgaard, P., Persson, M.: J. Phys. Condens. Matter **12** (2000) L13.
00Jo1 Jo, S., Gotoh, Y.: Surf. Sci. **464** (2000) 145.
00Jo2 Jo, S., Gotoh, Y., Nishi, T., Mori, D., Gonda, T.: Surf. Sci. **454** (2000) 729.
00Kel Kellogg, G.L., Plass, R.: Surf. Sci. **465** (2000) L777.
00Kim Kim, S.K., Kim, J.S., Han, J.Y., Seo, J.M., Lee, C.K., Hong, S.C.: Surf. Sci. **453** (2000) 47.
00Kis Kishi, K., Oka, A., Takagi, N., Nishijima, M., Aruga, T.: Surf. Sci. **460** (2000) 264.
00Kno Knorr, N., Brune, H., Epple, M., Hirstein, A., Schneider, A.M., Kern, K.: (2000) to be published.
00Kol Kolaczkiewicz, J., Bauer, E.: Surf. Sci. **450** (2000) 106.
00Kon Konvicka, C., Jeanvoine, Y., Lundgren, E., Kresse, G., Schmid, M., Hafner, J., Varga, P.: Surf. Sci. **463** (2000) 199.
00Kos Koschel, H., Held, G., Steinrück, H. P.: Surf. Sci. **453** (2000) 201.
00Lee Lee, A.F., Wilson, K., Lambert, R.M.: Surf. Sci. **446** (2000) 145.

00Lin Linderoth, T.R., Horch, S., Petersen, L., Helveg, S., Schønning, M., Lægsgaard, E., Stensgaard, I., Besenbacher, F.: Phys. Rev. B **61** (2000) R2448.
00Lin Ling, W.L., Takeuchi, O., Ogletree, D.F., Qiu, Z.Q., Salmeron, M.: Surf. Sci. **450** (2000) 227.
00Los Losch, A., Niehus, H.: Surf. Sci. **446** (2000) 153.
00Mar Markovic, N.M., Lucas, C.A., Climent, V., Stamenkovic, V., Ross, P.N.: Surf. Sci. **465** (2000) 103.
00Moo Moore, D.P., Ozturk, O., Schumann, F.O., Morton, S.A., Waddill, G.D.: Surf. Sci. **449** (2000) 31.
00Mró Mróz, S., Jankowski, Z., Nowicki, M.: Surf. Sci. **454-456** (2000) 702.
00Oni Onishi, H., Sakama, H., Aruga, T., Kawazu, A., Iwasawa, Y.: Surf. Sci. **444** (2000) 7.
00Osi Osing, J., Murphy, S., Shvets, I.V.: Surf. Sci. **454-456** (2000) 280.
00Pas Passeggi, M.C.G., Prieto, J.E., Miranda, R., Gallego, J.M.: Surf. Sci. **462** (2000) 45.
00Pen Pentcheva, R., Scheffler, M.: Phys. Rev. B **61** (2000) 2211.
00Pia Piaszenski, G., Göbel, R., Jensen, C., Köhler, U.: Surf. Sci. **454-456** (2000) 712.
00Pol Politi, P., Grenet, G., Marty, A., Ponchet, A., Villain, J.: Phys. Rep. **324** (2000) 271.
00Pri Prieto, J.E., Rath, C., Heinz, K., Miranda, R.: Surf. Sci. **454-456** (2000) 736.
00Ram Ramstad, A., Raaen, S., Barrett, N.: Surf. Sci. **448** (2000) 179.
00Rep Repp, J., Moresco, F., Meyer, G., Rieder, K.H., Hyldgaard, P., Persson, M.: Phys. Rev. Lett. **85** (2000) 2981.
00Sch1 Schaefer, B., Nohlen, M., Wandelt, K.: Surf. Sci. (2000) in press.
00Sch2 Schieffer, P., Hanf, M.C., Krembel, C., G, G.: Surf. Sci. **446** (2000) 175.
00Shu Shutthanandan, V., Saleh, A.A., Smith, R.J.: Surf. Sci. **450** (2000) 204.
00Töl Tölkes, C., David, R., Krzyzowski, M.A., Zeppenfeld, P.: Surf. Sci. **454-456** (2000) 741.
00Var Vargoz, E., Rusponi, S., Boragno, C., Kern, K., Brune, H.: (2000) to be published.